Graduate School ETD Form 9
(Revised 12/07)

PURDUE UNIVERSITY
GRADUATE SCHOOL
Thesis/Dissertation Acceptance

This is to certify that the thesis/dissertation prepared

By Muller Mark Soliman

Entitled
Developing a Neural Signal Processor Using the Extended Analog Computer

For the degree of Master of Science in Biomedical Engineering

Is approved by the final examining committee:

Ken Yoshida
Chair

Russell Eberhart

Jonathan Mills

To the best of my knowledge and as understood by the student in the *Research Integrity and Copyright Disclaimer (Graduate School Form 20)*, this thesis/dissertation adheres to the provisions of Purdue University's "Policy on Integrity in Research" and the use of copyrighted material.

Approved by Major Professor(s): Ken Yoshida

Approved by: Edward Berbari 07/06/2012
Head of the Graduate Program Date

Graduate School Form 20
(Revised 9/10)

PURDUE UNIVERSITY
GRADUATE SCHOOL

Research Integrity and Copyright Disclaimer

Title of Thesis/Dissertation:

Developing a Neural Signal Processor Using the Extended Analog Computer

For the degree of Master of Science in Biomedical Engineering

I certify that in the preparation of this thesis, I have observed the provisions of *Purdue University Executive Memorandum No. C-22,* September 6, 1991, *Policy on Integrity in Research.**

Further, I certify that this work is free of plagiarism and all materials appearing in this thesis/dissertation have been properly quoted and attributed.

I certify that all copyrighted material incorporated into this thesis/dissertation is in compliance with the United States' copyright law and that I have received written permission from the copyright owners for my use of their work, which is beyond the scope of the law. I agree to indemnify and save harmless Purdue University from any and all claims that may be asserted or that may arise from any copyright violation.

Muller Mark Soliman

Printed Name and Signature of Candidate

07/13/2012

Date (month/day/year)

*Located at http://www.purdue.edu/policies/pages/teach_res_outreach/c_22.html

DEVELOPING A NEURAL SIGNAL PROCESSOR USING THE EXTENDED ANALOG COMPUTER

A Thesis

Submitted to the Faculty

of

Purdue University

by

Muller Mark Soliman

In Partial Fulfillment of the

Requirements for the Degree

of

Master of Science in Biomedical Engineering

August 2012

Purdue University

Indianapolis, Indiana

ACKNOWLEDGMENTS

I would never have been able to finish my thesis without the guidance and the help of my committee members, and support from my family and friends.

First and foremost, I would like to express my deepest gratitude to my academic advisor Dr. Ken Yoshida for providing excellent academic guidance and for patiently editing my writing and supporting the research financially. More thanks go to Dr. Yoshida for his encouragement to overcome all obstacles in the completion this research work.

Moreover, I would like to thank my committee members, Dr. Jonathan Mills and Dr. Russell Eberhart for their valuable suggestions. Special thanks go to Bryce Himebaugh for developing the EAC prototype and updating the firmware to drive and test the matched filter. I would also like to thank my colleague in the Bioelectronics Lab, Shaoyu Qiao for his guidance and help in preparing of my thesis.

I would also like to thank my parents, Mark and Nagwa Soliman, and my siblings, Mayer, Mario, and Merna Soliman for always supporting and encouraging me with their best wishes and prayers.

Finally, I gratefully acknowledge the Indiana University Collaborative Research Grant (IUCRG) program for funding this research project and making this work possible.

TABLE OF CONTENTS

Page

Page

LIST OF FIGURES

Figure Page

Figure Page

Figure Page

ABSTRACT

Soliman, Muller Mark. M.S.B.M.E., Purdue University, August 2012. Developing a Neural Signal Processor Using the Extended Analog Computer. Major Professor: Ken Yoshida.

Neural signal processing to decode neural activity has been an active research area in the last few decades. The next generation of advanced multi-electrode neuroprosthetic devices aim to detect a multiplicity of channels from multiple electrodes, making the relatively time-critical processing problem massively parallel and pushing the computational demands beyond the limits of current embedded digital signal processing (DSP) techniques. To overcome these limitations, a new hybrid computational technique was explored, the Extended Analog Computer (EAC). The EAC is a digitally configurable analog computer that takes advantage of the intrinsic ability of manifolds to solve partial differential equations (PDEs). They are extremely fast, require little power, and have great potential for mobile computing applications.

In this thesis, the EAC architecture and the mechanism of the formation of potential/current manifolds was derived and analyzed to capture its theoretical mode of operation. A new mode of operation, resistance mode, was developed and a method was devised to sample temporal data and allow their use on the EAC. The method was validated by demonstration of the device solving linear differential equations and linear functions, and implementing arbitrary finite impulse response (FIR) and infinite impulse response (IIR) linear filters. These results were compared to conventional DSP results. A practical application to the neural computing task was further demonstrated by implementing a matched filter with the EAC simulator and the physical prototype to detect single fiber action potential from multiunit data streams derived from recorded raw electroneurograms. Exclusion error (type 1 error) and inclusion

error (type 2 error) were calculated to evaluate the detection rate of the matched filter implemented on the EAC. The detection rates were found to be statistically equivalent to that from DSP simulations with exclusion and inclusion errors at 0% and 1%, respectively.

1. INTRODUCTION

1.1 Background

The human nervous system is one of the most complex systems in the body. Among its functions is to establish two-way communication between the brain and organs, as well as interpret and act upon ascending and descending signals, i.e. signals from the periphery to the brain, and signals from the brain to the periphery, respectively. Attempting to understand the communication pathway has been an interesting topic for several researchers through the ages. Our curiosity has driven investigation of this through the centuries, isolating the locus of consciousness to the mind; to the nervous system. In other words, consciousness is translated by information that is transmitted and processed by the nervous system. If we accept this hypothesis to be true, then in essence, everything that we do to the environment and everything that we perceive from the environment is mediated through the nervous system. Observing and understanding the information flow is the gateway to understanding the human experience.

The peripheral nervous system (PNS) plays an important part in the transmission of information and the transduction of information to/from the environment. It can be thought of as the body's wiring connecting the brain and central nervous system (CNS) to the sensors and actuators (muscles) located throughout the body. Like a bundle of telephone wires, the peripheral nerve consists of bundles of nerve fibers. Each fiber within the nerve fascicle is hardwired from its cell body in the CNS to its end organ in the periphery. The information it transmits corresponds one to one to the information directed to/from that end organ. We refer to this unitary fiber as a single unit in the nervous system. The nerve fibers are bundled topologically together into nerve fascicles, and nerve fascicles are bundled together to form nerve trunks.

The information transmitted in the nerve fiber only flows in one direction: Sensory fibers only conduct information from the sensory end organ centrally to the CNS. Motor fibers only conduct information from the motor regions of the spinal cord peripherally to the muscle. These sensory and motor fibers are typically mixed within nerve fibers. Information is transmitted down the nerve fiber by taking advantage of the bioelectric phenomenon taking form in a self-propagating impulse that travels down the nerve fiber, the action potential (AP). By itself, the AP does not contain any information, but is rather, akin to the carrier wave the information. The body encodes magnitude using two schemes, rate coding and population coding [1]. Within the single fiber, magnitude information is encoded as the frequency of the action potentials traveling down the fiber. Thus, the information in the nervous system is transmitted digitally, in a schema akin to pulse code modulation used in digital electronic communication. These firing patterns of each single fiber, extracted from the multiunit recordings, provide feedback control in functional neuromuscular stimulation systems [2]. Therefore, we are in need of a device that is capable of monitoring neural activity and perform signal processing in real-time.

1.1.1 Neural Interfaces

The bioelectric phenomenon is central to much of what we know about the nervous system. We are able to detect minute electrical potential disturbance caused by the transit of APs through electrodes placed on or within the neural tissue. The technique of capturing signals of neural origin is collectively called Electroneuronography (ENG). Similarly, APs originating from the bioelectrical activity of other tissues form the basis for electromyography (EMG) for skeletal muscles, electrocardiography (ECG) for cardiac muscle fibers, electroencelphalography (EEG) for the brain, electrocorticography (ECoG), etc. These extracellular potentials of the single nerve fiber range in magnitude from 1 μV through $\sim$ 100 μV in amplitude, and approximately

1 ms in duration. The frequency content of the single fiber action potential (SFAP) ranges up to several kilo Hertz to tens of kilo Hertz [3] [4].

Although the geometry of the neural interface plays a major role in its ability to detect single unit activity, given a selective electrode placed within the nerve tissue, the amplitude and frequency of the single units are altered in shapes depending on the location and direction of the electrode in addition to the conduction velocity of SFAP [5] [6] [7] [8]. It was proposed that the rate of a sufficient number of recorded units could supply information regarding joint position, skin indentation, muscle length and tension, etc [9]. Therefore, detecting and classifying these SFAP units based on shapes are the ultimate techniques to decode the contained information in the neural data stream.

Given a sufficiently selective electrode, the nerve fibers are resolved as spike waveforms within the recording. These spikes have unique shapes resulting from the unique path that each nerve fiber takes with respect to the recording electrode position. The activities of more distant fibers are smaller in amplitude and interfere with one another, contributing to the amplitude of the background noise [5]. They are further contaminated by environmental noise such as line noise and pickup of other bioelectrically active tissues.

Detecting and classifying SFAP patterns in the digital signal processing (DSP) environment may be a difficult task due to the massive computations that need to be performed in a short period of time. The processing that is currently performed off-line amounts to detecting and identifying different nerve fibers based on differences in the shapes of the units measured by the electrode. To sufficiently sample the shape and the noise overlying the signal, the potential from each electrode contact is typically sampled at a rate of between 30 and 50 kHz to provide adequate oversampling [10]. Current peripheral neural interfaces contain between 8 and 16 active contacts [11] making the aggregate sampling rate needed approaching 1 MHz. Several more operations need to be performed for the denoising, detection, and classification phases. For example, to design a 32-sample matched filter to detect SFAP in

a multiunit recording, about 130 operations need to be performed for each contact in the electrode. This indicates that more than 20,000 operations need to be performed before moving to the next sample, $\sim 20\ \mu s$. If principal component analysis (PCA) was then used to classify the detected SFAPs with two principal components that have the largest variance values along with Euclidean distance calculations to cluster the units, at least 500 more operations need to be performed for each contact in the electrode. This would require another 80,000 operations per $\sim 20\ \mu s$. However, today's state-of-the-art DSP devices such as TI TMS320C6 series can only perform up to 55,000 operations in the 20 μs period at full speed (2746 mega floating-point operations per second) [12].

Therefore, hundreds of DSP devices in a multicore high performance computer are necessary for the parallel computations so that the single units can be detected in each channel fairly quickly in real-time. Power computation in DSPs is achieved by constructing higher level functions at the expense of clock cycles which comes from switching states on the gates, so that high performance in terms of speed comes at the cost of greater power consumption. An additional constraint is the time-critical nature of the information. Signal processing, control and activation of the system must be conducted so that the total processing and system delay do not exceed a few milliseconds and become noticeable to the user. Additional delays would not only slow down the system, but also have the potential of impacting the system stability. Therefore, the need of a low power, portable and powerful computational signal processor tool still exists. This document aims to address this problem by applying a new computing technique, the extended analog computer, to address the technological gap for mobile neural signal processing.

1.1.2 The Extended Analog Computer

The extended analog computer (EAC) is an analog computing paradigm that was first proposed by L. A. Rubel in 1993 [13]. It was envisioned to take advantage of the

intrinsic computational power of distribution of potentials in space. Originally, Mills et al., created a device consisting of a conductive sheet and a matrix of contacts, bounded by insulated boundaries [14]. It can be described as a uniform volume conductor with Neumann boundaries and a regular array of input/output contacts. Each contact could be configured as a current source or current sink. Current sources were defined as the set of inputs to the computer, and current sinks as the outputs. Each output was processed through a restricted set of piecewise linear logic functions, Lukasiewicz logic arrays (LLAs), and could be routed back onto the original sheet (recursion), or routed as an input to another sheet. Particle Swarm Optimization (PSO), an artificial machine learning optimization technique invented by Kennedy and Eberhart [15], was used to train the connections and LLA set to train and configure the EAC. These devices were successfully used in various applications such as in prediction of the folding of proteins and character recognition [16]. Thus, the EAC was an attractive technology to be developed into other forms of analog neural signal processing.

1.1.3 History of the EAC

Modern electronic analog computers were invented before electronic digital computers [17]. The first analog computers were designed to solve ordinary differential equations especially in Ballistics problems in military in the forties and fifties in various applications such as gunfire control and aircraft design [17]. The General Purpose Analog Computer (GPAC) was first introduced by Shannon in 1941 [18], and refined by Pour-El and then Lipshitz and Rubel [19] [20]. The GPAC was described as a mathematical model of analog device that consists of a finite number of analog units. It was first built with mechanical components and then evolved to electronic versions. This device was designed to do linear computations in real-time such as summation, multiplication, and simple integration. It can also simulate Turing ma-

chines [21], which are the first Logical Computing Machines invented in 1937 by Alan Turing [22].

Rubel believed that the GPAC was unable to solve many problems to implement the functions of decision-making processes in the human brain because of the non-linearity functions [23]. Therefore, Rubel created a new theoretical model of multi-dimensional sensory inputs in uncertain decision processes (EAC) with LLA implementation to perform non-linear functions. This architecture was further developed and implemented by Mills and colleagues at Indiana University Bloomington in 1995. The EAC developed was a restricted version of the Extended Analog Computer based on sampling electric current or voltage distribution in a sheet of electrically conductive foam. Unlike the GPAC, the EAC was simple but yet proved to be able to compute solutions to complex problems [24].

1.1.4 Why the EAC?

The EAC has demonstrated the potential to make massive instantaneous, parallel computations while consuming very little power to make those calculations [24]. Moreover, the principles of the device allow it to be miniaturized through microfabrication techniques to create a portable, massively parallel, computational platform. Such properties are extremely attractive for development of small, implantable, or autonomous remote devices that require high performance computing, where massively parallel massively multi-core DSP is not a realistic option, such as a future neural signal processor.

In its original version, the Mills implementation of the EAC was defined as a current-current device, where the inputs were current sources and the outputs were current sinks. The locations of these current sources and sinks modified the current density manifold. Thus, the EAC could be configured to solve specific spatial partial differential equations by configuring the location and current gain of the set of input sources and sinks, adjusting the current density manifold to solve the problem. As

such, the device was well suited for automatic machine learning and optimization technique, which automatically adjusted the location of the inputs and outputs to result in the optimal configuration to solve a particular problem. However, the manifold of the current density mode is not well suited for input functions that are time-varying, such as the raw time-varying recordings coming from a neural prosthetic interface. This is because the current density manifold is not independent of the magnitude of the set of currents injected into the volume conductor. The Neural Signal Processing problem needs a stationary manifold acting on a time-varying input data stream.

1.2 Problem Statement

The GPAC and EAC are capable to solve linear spatial problems that include different operations such as multiplication and integration. But, we hypothesize that it can be adapted so that it performs the same computations in the time domain for real-time neural processing. It can be adapted to solve linear differential equations in real-time as efficient as DSP devices using low power. Arbitrary any-order Finite Impulse Response (FIR) and Infinite Impulse Response Filter (IIR) can be implemented where their qualities are equivalent to DSPs. This hypothesis is validated by implementing a matched filter, a practical application of an FIR filter, with the EAC and compared to a DSP simulation of the same filter to give evidence for our hypothesis.

The aim of the present work was to modify and develop the EAC to accept time-varying inputs, and determine the governing equations of the new mode of manifold computing. We develop the Potential Manifold paradigm, resistance mode, for Extended Analog Computing. We describe a means to enable the EAC to accept sampled temporal data streams, and develop, through the use of reciprocity arguments, a method to analyze the governing equations of the voltage manifold. We explore the effects of volume conductor, input/output site geometry and conductivity on these governing equations. The method was validated through demonstration of equality

to analytical solutions, and through the implementation of arbitrary FIR filters and IIR filters. Furthermore, A matched filter designed to detect the presence of a known ENG single unit was developed to show proof of principle of the application of the EAC to detect neural units within a neural data stream.

1.3 Organization of the Thesis

Chapter 2 presents a general analysis of the EAC and an explanation of the resistance mode that was developed. This chapter explains the theory and analytical solution of the potential manifold due to one or multiple current sources. Additionally, it describes the effect of insulated boundaries and their benefits to maintain low power and higher potential in the meantime. Various shapes of current sources were also analyzed to reach an optimized shape that is easy to manufacture and give precise results that match the analytical solutions.

Chapter 3 describes a new method developed to map and process time varying signals onto the EAC. It describes the use of the reciprocity theorem to analyze the filters weighting function and its link with time to apply different types of FIR filters. It also demonstrates a fixed-location configuration of the EAC to implement 8-bit resolution weights of arbitrary FIR filters. This chapter also emphasizes the medium thickness effect of the EAC on filtering and the possibility to change the thickness without affecting the manifold distribution. Moreover, the capability of building a high-order FIR-IIR filter is demonstrated with an example.

Chapter 4 demonstrates the application of the EAC to process neural signals. The procedure of implementing a matched filter for detection and identification of single unit spikes in a multi-unit recording is described. This chapter also proves that the quality of EAC is equivalent to the quality of DSPs. This is done by comparing the matched filter results by three different systems: digital signal processor, EAC resulting from finite element method (FEM) model, and EAC resulting from a developed

physical prototype. In addition, low exclusion and inclusion errors were calculated by testing the system with a synthesized neural activity.

Chapter 5 gives a discussion of all parts of the thesis. It also discusses some ideas about possible research in the future in order to have a fully developed EAC that can then be implanted. Then, the summary section summarizes the work done in this thesis.

2. REANALYSIS OF THE EAC

The starting point of this work was the Extended Analog Computer platform developed by Mills et al., the μEAC R002, shown in Fig. 2.1 [14]. The device is a macro sized demonstrator of the technology and consists of a set of 25 points contacting a 12 $cm \times 12\ cm \times 0.5\ cm$ conductive foam in a regular 5×5 matrix. Each point can be configured as a voltage source, current source/sink or voltage/current measurement point by driver control software running on a desktop or laptop personal computer. Current density and potential manifold are formed on the conducive foam.

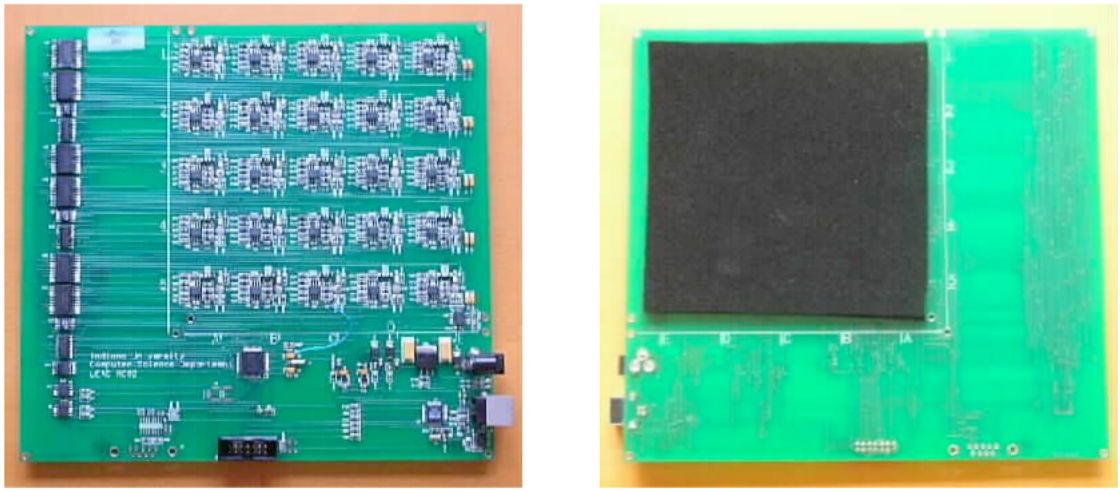

Fig. 2.1. The μEAC R002 developed by Mills et al. [14]. The black material that exists at the bottom of the μEAC R002 is the conductive foam where current density and potential manifold are formed.

The device was designed to be configured via machine learning and automatic optimization techniques to predict a solution to a multidimensional problem posed as to a static, spatial problem projecting to the 25 points. The aim of the present

project was to modify and configure this static, spatial processor to enable processing of inputs that are variable in time. It was realized that the volume conductor itself intrinsically distributes the current density as a solution to Laplace and Poisson's equations, and that this solution can be monitored by measuring the current density or potential manifold at specific points on that distribution. Moreover, the manifold can be conditioned by the addition and positioning of current/voltage sources and sinks to solve arbitrary partial differential equations. An understanding of the mechanism of how the voltage/current density manifold forms on the volume conductor, how the boundary conditions influence that manifold, and how solutions to differential equations form within the volume conductor was necessary before the device could be modified to address the neural signal problem we posed to it.

In this chapter the formation of the potential manifold within the volume conductor is analyzed. Next, a method to deterministically configure and sample the manifold to perform arbitrary linear operations and solve partial differential equations of time is developed.

2.1 A Black-box Analysis and the Possible EAC Modes of Operation

In the concept of the EAC the positions of a multiplicity of the sources and sinks are placed to condition the voltage/current manifold to solve specific PDEs. These sources and sinks can be defined as either electric currents or voltages, and the manifold voltage or current can be monitored. Therefore, there are four possible source/sink and voltage/current monitoring combinations in the active input / passive output case. These can be conceptually described in terms of a black-box two-port network analysis of electric devices.

The two-port network is a simple circuit or device that has two pairs of terminals (two inputs and two outputs) and was first introduced in the 1920s [25]. It can be treated as a black box represented by four different variables: I_1, V_1, I_2, and V_2 which denote input current, input voltage, output current, and output voltage, respectively

as shown in Fig. 2.2. For any two-port network, the relationship between these variables describes its characteristics.

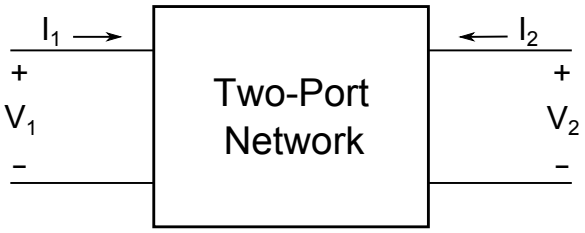

Fig. 2.2. A schematic representation of a two-port network.

In the general two-port black-box, the output port is a function of the signal exciting the input port and vice versa. Thus, several configurations of the two-port network can be considered where the three main categories are active/active, active/passive, and passive/active input/output. For the active input port, electric current or voltage is applied and for the passive output port, electric current or voltage is measured. This leads to eight different configurations of the two-port model can be considered, shown in Fig. 2.3. However, in the EAC, active input and passive output ports are always considered, which indicates that the input port is not affected by the output port. Therefore, only four modes of operation are considered. These four possible modes that the EAC can be operated in are current gain, voltage gain, resistance, and conductance mode.

The EAC is capable of working in as many as four different two-port networks where no electric current or voltage are applied at the output port. These configurations are shown in Fig. 2.4. In the current gain mode, both input sources and output measurements are electric currents. This leads to high input impedance, but low output impedance. Therefore, when more output measurements are introduced to the system, potential manifold is altered. This mode was explored by Mills et al. for different applications such as protein folding and machine learning techniques. In the voltage gain mode, both inputs and outputs are voltages. This leads to low

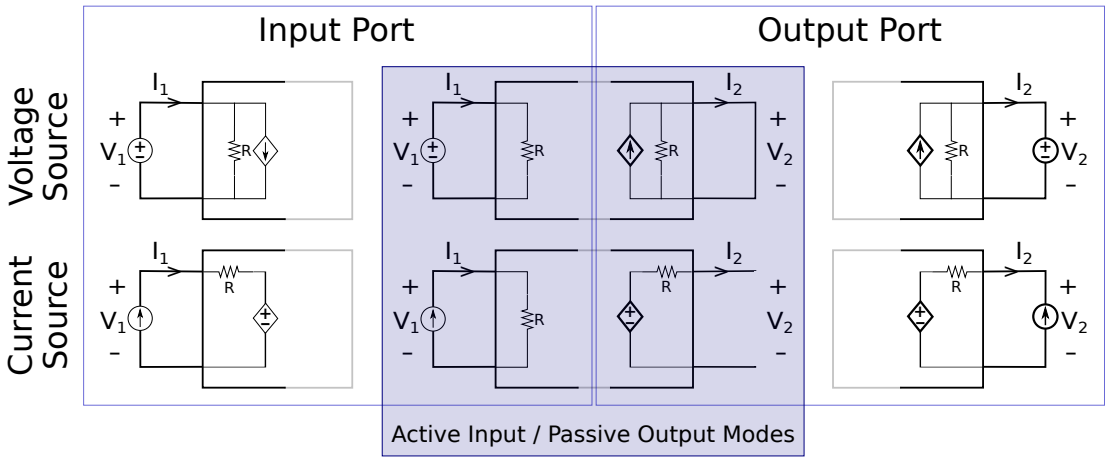

Fig. 2.3. Schematics of all possible two-port model configurations. The four highlighted schematics (two input and two output ports) represent the four possible combinations of active input / passive output modes of operation that the EAC can be configured into.

input impedance, but high output impedance. In this case, the manifold is modified and current sources are not independent of each other. Unlike the other modes, high input and output impedances occur in the resistance mode where input sources are currents and output measurements are voltages. In this case, all inputs and outputs are independent of each other. In the opposite case, both inputs and outputs are not independent of each other in the conductance mode, where input sources are voltages and outputs are currents.

The EAC conceptualized by Mills et al. was originally defined as a current gain device, where the inputs were current sources and the outputs were current sinks [26]. The locations of these current sources and sinks alter the current density manifold in the volume conductor. Then, specific partial differential equations can be solved by arranging the source/sink locations. However, when more inputs or outputs are introduced to the volume conductor, the current density in the volume conductor is no longer stationary. Additionally, the magnitude of input currents changes the current density manifold in the volume conductor. Thus, the manifold itself is not

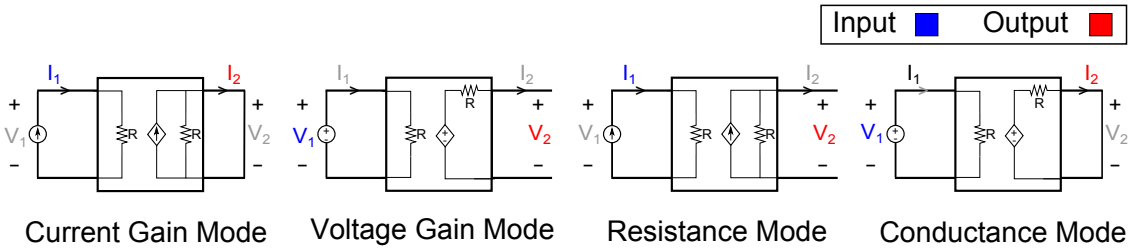

Fig. 2.4. Schematics of the four different modes of operation of the EAC: current gain, voltage gain, resistance gain, and conductance mode.

stable, changing PDE solutions depending upon the relative input magnitudes. So, for time varying inputs, this mode does not result in a stable solution manifold. The same situation is true in the voltage gain mode where both inputs and outputs of the system are voltages.

In contrast, in the case of the resistance mode, the current source and voltage measurement are defined to have infinite output impedance and infinite input impedance, respectively. Consequently, the potential distribution created by current sources in the conductive space are independent of each other. Thus, the manifold changes as the sum of the solutions of each individual input. Thus, additional inputs only add complexity to the mathematical expression without influencing the other inputs. Moreover, additional voltage detection measurements do not alter the potential manifold. Similarly, additional inputs do not influence other inputs in the conductance mode where inputs are represented by voltages and outputs are represented by electric currents. Measuring voltages however is more suitable than measuring electric currents.

Therefore, in the resistance mode, it is possible to take advantage of the independence of measurement and additional input source. The principle of superposition can be applied in the resistance mode simplifying the analysis of the potential distribution in the manifold space.

2.1.1 The EAC in the Resistance Mode

Potential manifold is mapped onto a conductive medium when a current source is injected into it as long as there is at least one sink point to allow current path in the medium. Source/sink pair locations alter the potential distribution in the volume conductor, along with the boundary conditions imposed at the extent of the medium. The homogeneous resistive volume conductor can be thought of as a fully connected 3-D lattice of resistors. An equivalent to the volume conductor in 1-D is the resistive network, which has been used as part of an Analog Computer, and currently is used in various high speed mathematical applications. An example of this is an R-2R ladder circuit which is made of repeated network of resistors, which is used to perform flash digital to analog conversion, as shown in Fig. 2.5.

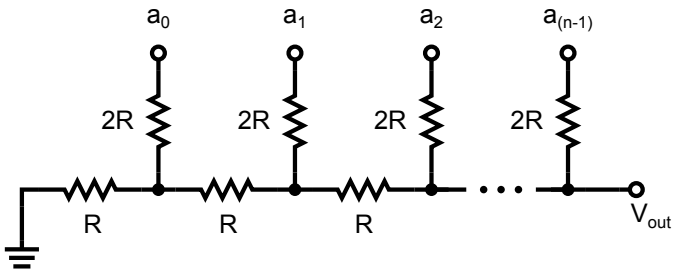

Fig. 2.5. A schematic of an n-bit R-2R resistor ladder circuit.

The EAC can be thought of as an extension of this 1-D case to the 3-D case, where the potential distribution that develops in the space is used to solve 2 or even 3-D solutions of PDEs. To understand what the EAC manifold can solve, it is necessary to understand how the distribution of current densities and potentials form in the space and how boundaries, source/sink location and geometries influence the potential manifold. Finite element simulation of the EAC manifold was used in this thesis as a means to explore how different conductive media and their configurations influenced the EAC manifold. The foundations of the FEM technique and analog

simulations of a conductive space as they relate to analog computing are described in [27]. These will be described in the next section.

2.2 Early Work in Analogue Computing and the Resistance Network

Analogue computing devices were proposed prior to the 19^{th} century to solve mathematical problems defined by geometric relationships [28]. The development of the first direct electrical analogue techniques such as the electrolytic tank and the conducting paper were designed to perform computations in the solution of boundary value problems and operate on a principal known as field analogy. In the 1870s, the British scientist, William Adams, published the description and use of the electrolytic tank solving field equations [29] [30]. The apparatus is an analogue model of the electric field distribution in dielectrics and consisted of a wooden tank containing a conductive solution (water), two fixed metal electrodes, and two mobile electrodes [31]. The German physicist, Gustav Robert Kirchhoff, used a conductive sheet of copper to explore the potential distribution in an electric field [27]. The conductive sheet works as a three-dimensional series of resistors (resistance network) as explained later.

The foundation of analog simulations by a conductive space that is represented by a resistance network was explored by Karplus [27]. DePackh and Redshaw presented their first published reports of successful solutions of Laplaces and Poissons equation by the resistance network technique [32] [33]. The field is distributed in a continuous manner throughout the conductive material; therefore, finite-difference approximation was employed to understand the underlying equations of potential distribution in the conductive space. If we considered a one-dimensional continuous conductive system (Fig. 2.6A), then the field can be mathematically discretized by a series of network resistors (Fig. 2.6B) that replaces the continuous system. Then, finite-difference approximation is applied to determine the governing equation (Fig. 2.6C).

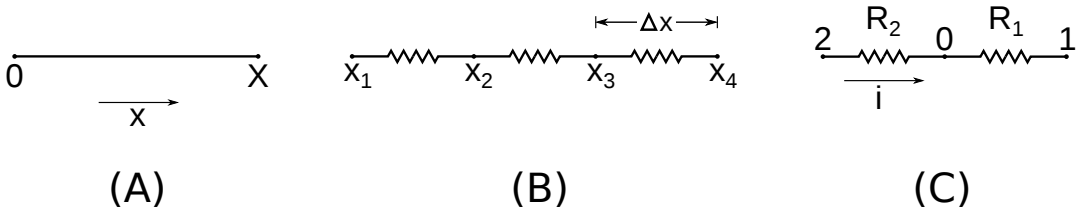

Fig. 2.6. (A) One-dimensional continuous conductive system. (B) Discretized equivalent representation of (A). (C) differential element approximation.

As shown in Fig. 2.6, the wire has been replaced by n (3) resistors. Then, x coordinate is specified as discrete steps x_1, x_2, $\cdots$. If the resistivity of the wire is ρ *ohms* per unit length and the spacing between the resistor nodes is Δx, each resistor must have a value of $\rho\ \Delta x$ *ohms*. According to the continuity principal, the current passing through the resistors R_1, R_2, and nodes 0, 1, and 2 (see Fig. 2.6C) are the same. And according to Kirchhoffs current law where R_1 and R_2 are equal

$$V_1 - 2V_0 + V_2 = 0 \tag{2.1}$$

This equation is the finite-difference approximation of the one-dimensional partial differential equation (Laplace's equation)

$$\frac{\partial^2 V}{\partial x^2} = 0 \tag{2.2}$$

Subsequently, the three-dimensional conductive space is the discretized approximation of the Laplace's equation in three-dimensions and represented by the following equation

$$\frac{\partial^2 V}{\partial x^2} + \frac{\partial^2 V}{\partial y^2} + \frac{\partial^2 V}{\partial z^2} = 0 \tag{2.3}$$

The solution of field problems by means of resistance networks was described by Karplus in the 1950s by the following points [27]. The field is modeled as a network

of large number of electrical resistors where all resistors have the same value in case of homogeneous isotropic conductive space, as shown in Fig. 2.7. The voltage or current sources are then applied to the resistance network at its external boundaries and the interior nodes. The potential distribution is then determined by measuring and recording the voltage at each node of the network. The equipotential lines and streamlines are then sketched by interpolating between points of measured potential. Accurate and precise solution is achieved with a higher density of resistors per unit volume. Finer net spacing is sometimes necessary in cases where a more accurate solution on the conductive space is needed and can be specially applied in the portions of the field in which the potential undergoes sharp variations. Therefore, diagonal nets are also considered so that every node is connected to all adjacent nodes in the cube block.

Finite difference is a numeric method that aims to approximate a solution to differential equations using finite different equations to approximate derivatives. Finite element is an equivalent method of finite difference, however, it approximates the solution of differential equations using integration and linear algebra techniques. Presently, the finite element method has become the most common modeling numerical technique in engineering. The power of the finite element modeling arises when considering complex geometries where the finite difference method becomes harder to implement and its demands of computational power increases. Therefore, a finite element method modeling package, COMSOL Multiphysics, was used in this thesis, where the meshing size is proportional to the density of resistor components per unit volume.

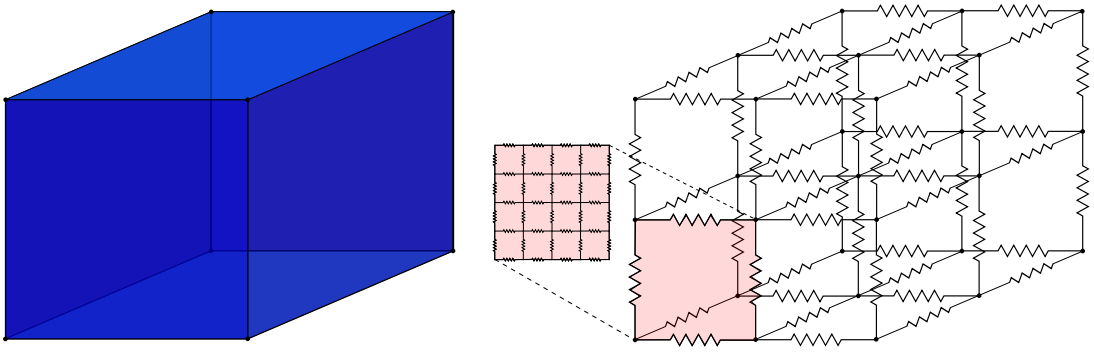

Fig. 2.7. Conductive space is modeled and approximated by a network of resistors that are fully connected where larger density of resistor components (less meshing size) gives more accurate potential distribution.

2.3 The Effect of the Neumann and Dirichlet Boundary Conditions

To understand the distribution of the potential manifold and the influences of boundaries, begin the analysis with a simple case of a dipole source/sink pair in a uniform, conducting volume, bounded by an insulator. This simple case is used since a known analytical solution exists, and Finite Element Model analyses which are conducted later for more constrained realistic volumes can be validated with the analytical solution. In this simple case (see Fig. 2.8) several observations can be made.

The current injection and sink points can be clearly seen as the red and blue points on the right and left half of the space, respectively. Two perpendicular lines of symmetry can be described. In one case, a line can be described bisecting the space into top and bottom (Fig. 2.8B). Likewise, another line can be described splitting the space into left and right sides (Fig. 2.8C).

In the case shown in Fig. 2.8B, the bottom and top sub-spaces are identical mirror images of one another. One can also observe that the current path is parallel to the horizontal symmetry line that passes through the source/sink pair. The horizontal symmetry line defines a mirror plane. Since the potential distribution at the top and

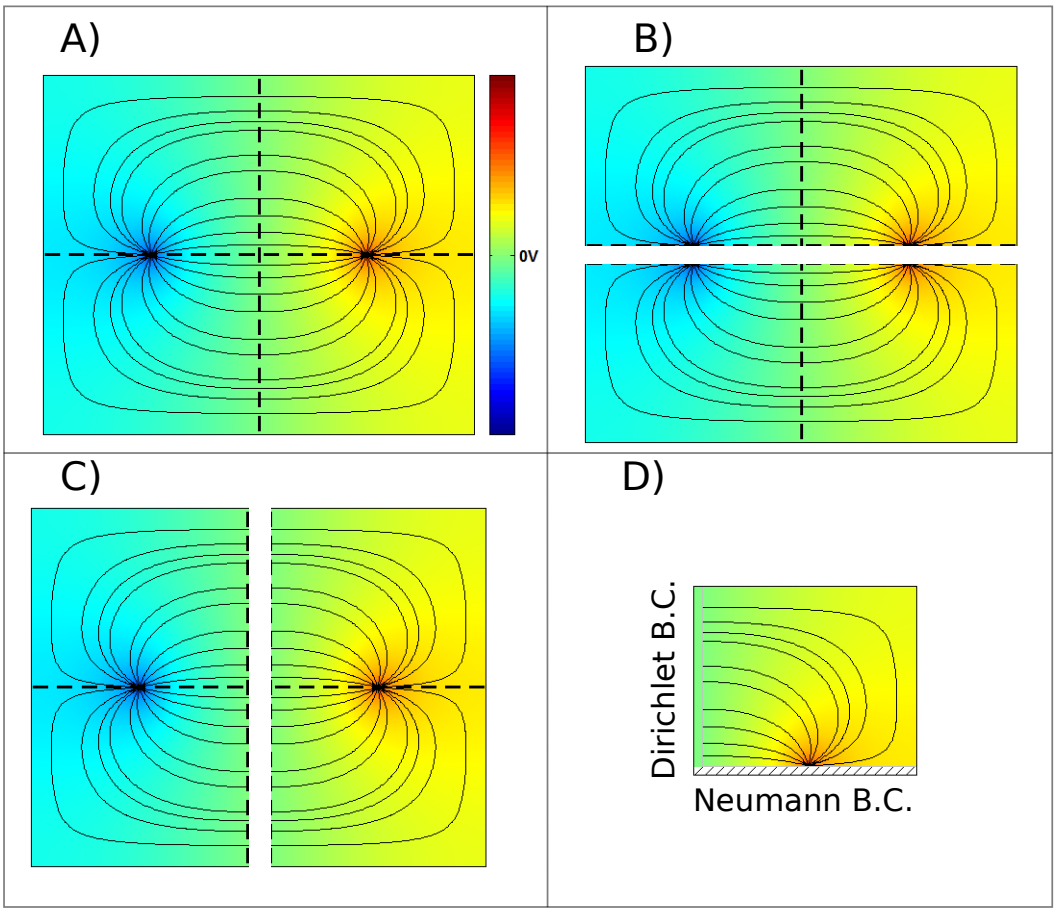

Fig. 2.8. (A) Potential distribution in a conductive medium due to a current source (right) and current sink (left) at which there are two symmetry lines. (B) The Potential distribution and current density of the bottom side of the horizontal symmetry line is a mirror image of the top. (C) The Potential distribution of the left side of the vertical symmetry line is an inverted mirror image of the right. (D) a quarter of the medium that represents the driven solution that is achieved by replacing the horizontal line by an insulated boundary (Neumann boundary condition) and the vertical symmetry line by a grounded boundary (Dirichlet boundary condition).

bottom sides are identical, only one side would give the desired solution. Therefore, an insulated boundary is applied at the symmetry line location so that half current magnitude and space volume are achieved. The insulated boundary condition reflects

the potential, and the current density flows parallel to it. This type of boundary is defined as a Neumann boundary condition [34] and is mathematically denoted with the following equation:

$$n \cdot \nabla \overline{J}\big|_{\Omega} = 0 \tag{2.4}$$

where n is the outward normal vector of the boundary Ω and $\overline{J}$ is the current density which is zero in the normal direction.

In the case shown in Fig. 2.8C, the left and right sides are inverted mirror images of one another. The vertical symmetry line defines a zero potential in case of equal source/sink values where the current path is perpendicular to that line. Therefore, only one of these sides gives the expected solution of all the medium. Thus, it was decided to reduce to half the area of this medium and ground the boundary at which the potential distribution and current density remain the same. The grounded boundary in this case can be mathematically modeled as a Dirichlet boundary condition which is the boundary condition at which the potential value is zero and current density flows perpendicular or normal to this boundary [34]. Mathematically, the Dirichlet boundary is denoted with the following equation:

$$\phi|_{\Omega} = C \tag{2.5}$$

where ϕ denotes the potential at the corresponding boundary Ω and C is a constant. For a grounded boundary, $\phi|_{\Omega} = 0$.

Therefore, modeling only a quarter of the medium gives the expected solution that is given at the whole medium with only half of the current magnitude. A grounded boundary, Dirichlet boundary condition, is implemented to replace a current sink and reduce the volume conductor by half. An insulated boundary, Neumann boundary condition, reflects the current as a mirror plane as explained later. It is implemented proximate to a current source to allow half the volume and half the current magnitude as well.

2.3.1 Analytical Solution of Potential Distribution

If we restrict the media to a homogeneous resistive volume conductor, the potential distribution in the volume resulting from a point current source in the volume drops as a function that is inversely proportional to the radius from the point source. Thus, the potential manifold resulting from a point current source is described by a function that is strictly related to the conductivity of the medium and inversely proportional to the radius; the function has a radial basis [35]. This relationship can be analytically described using the classical equations of electrostatics. Restated, if we consider a point current source of magnitude I in a uniform conductive infinite medium with conductivity of σ, equipotential (isopotential) lines must be uniformly circular where current flow lines are perpendicular to them and directed radially [36]. For a spherical medium with a radius of r, the current density $\overline{J}$ crossing this surface must be uniform and estimated by

$$\overline{J} = I/4\pi r^2 \tag{2.6}$$

From the field theory, it is known that the electric field $\overline{E}$ is related to potential ϕ by

$$\overline{E} = -\nabla\phi \tag{2.7}$$

Also, by Ohm's law

$$\overline{J} = \sigma\overline{E} \tag{2.8}$$

From Eq. 2.6, Eq. 2.7, and Eq. 2.8

$$I/4\pi r^2 = -\sigma\nabla\phi \tag{2.9}$$

And by integration with respect to r considering that the medium is isotropic where $\sigma_x = \sigma_y = \sigma_z = \sigma$, the potential field at r distance away from the current source can be estimated by

$$\phi = \frac{I}{4\pi\sigma r} \tag{2.10}$$

where $r = \sqrt{(x-x')^2 + (y-y')^2 + (z-z')^2}$, each monopole is located at (x, y, z), and the field point is at (x', y', z').

The potential distributions predicted by the analytical equations assume an infinite, uniform media with point sources. Differences in the source geometry, the shape of the volume conductor, and the boundary conditions will have an effect on the potential distribution, and thus the solutions given by the EAC. In these cases, it is not easy to determine analytical expressions to determine the potential distribution analytically. Therefore, a finite element method (FEM) model was implemented to analyze the behavior of the voltage manifold with different configurations. The sensitivity of the potential distribution solution to real constraints, and the effect of different irregular geometries were analyzed using the FEM technique. These models were implemented in Comsol Multiphysics 3.5a with the Conductive Media DC module (COMSOL Inc., Burlington, MA).

2.4 Analytical vs. Empirical Solution

The analytical solution of the potential field is based on the assumption that the medium is of infinite extent. This is practically not possible; however, grounded boundaries, Dirichlet Boundaries, with COMSOL 3.5a provide accurate and acceptable results in the first $\sim 90\%$ of the distance between a centric current source and the medium boundary while the current and potential distribution are distorted in the other $\sim 10\%$ due to the boundary conditions as shown in Fig. 2.9. In terms of the boundary constriction zone about 10% at each grounded side of the medium should not be used either for inputs nor detection points. This region is largely influenced by the boundary conditions and defined as the zone near a source or sink electrode of a current path [37] where the current density or potential distribution is dictated by the boundary condition. Fig. 2.10 shows a schematic of a conductive medium with 10%

restricted zone from the grounded boundaries. Equipotential lines that are within the restricted zone get distorted from the circular shape. The experimental results were simulated using a finite element modeling software, COMSOL 3.5a. The EAC computes based upon how the manifold changes as a function of the input sources. In other words, the potential distribution near the sources and the "near field" defines the EAC solution set. The boundaries at the extent of the volume conductor only serve as an approximation to an infinite volume conductor, a return path for the currents injected, and an approximation of the "far field". To a large extent, they do not enter into the computations that the EAC makes.

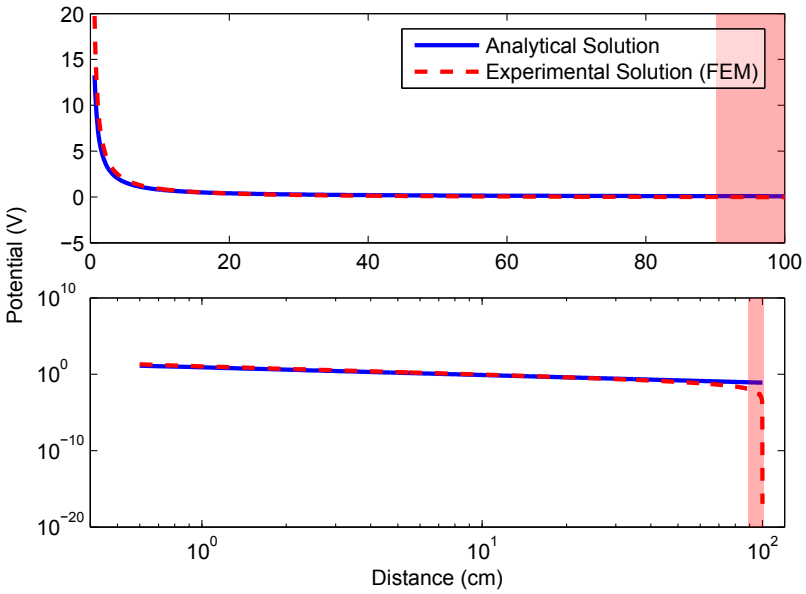

Fig. 2.9. A comparison between the potential distribution from the analytical and empirical solutions for a current input source in a conductive medium. The empirical solution was simulated with COMSOL 3.5a for a centered current point source of 1 A in a spherical medium with a radius of 1 m and conductivity (isotropic) of 1 S/m at grounded boundaries state.

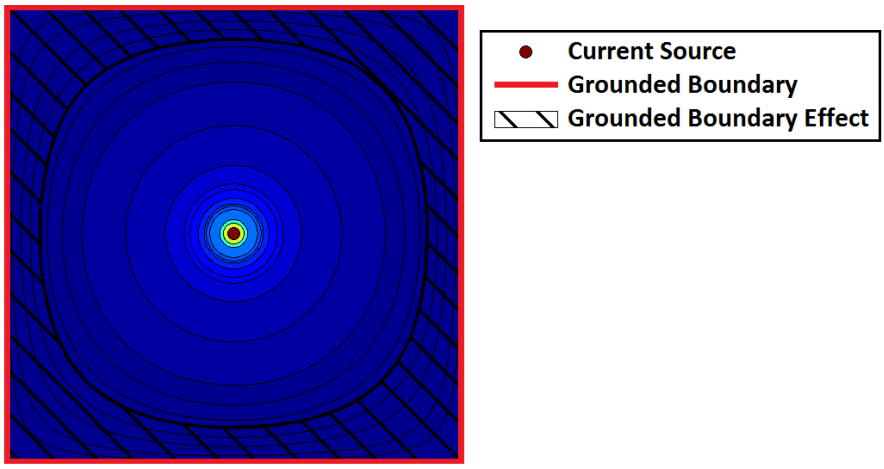

Fig. 2.10. A schematic of potential distribution and equipotential lines on a conductive medium with 10% restricted zone at all grounded edges that is influenced by the grounded edges.

2.5 The Superposition Principle

The distance between the current source and the voltage detection point is a major key in the EAC. As explained above, the reciprocal of the distance represents the coupling between the input and the detections point. Moreover, multiple inputs can be introduced to the medium and the potential at the detection point can be predicted using the superposition principles. The superposition principles are valid in the resistance and conductance mode, but not in the current or the voltage gain mode where the source/sink inputs and outputs alter the current density. The potential at the detection point is equivalent to the weighted sum which can be calculated by

$$\phi = \frac{1}{4\pi\sigma} \sum_{i=1}^{N} \frac{I_i}{r_i} \tag{2.11}$$

where σ is the medium conductivity, I_i is the injected current at current source i, r_i is the distance between the source i and detection point, and N is the number of current inputs.

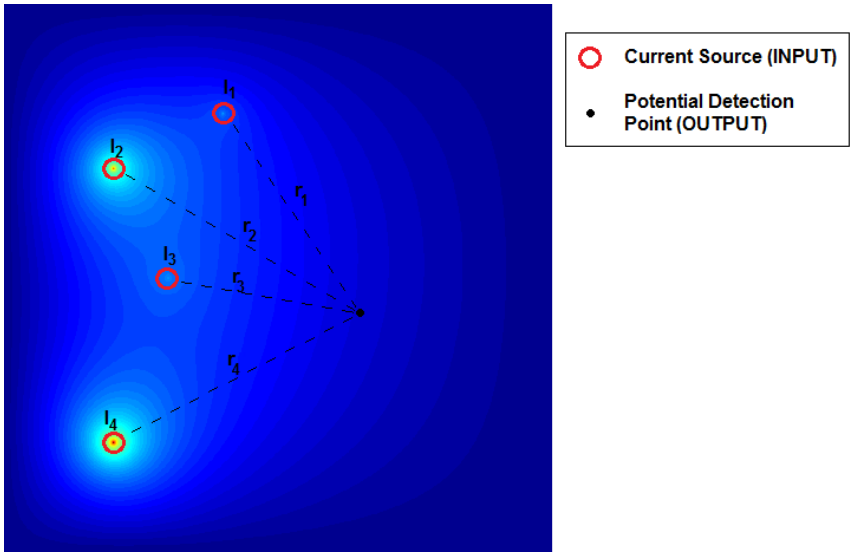

Fig. 2.11. A grounded boundaries conductive medium with four different point current sources at different locations and one potential detection point.

Fig. 2.11 shows an example of four current inputs in a conductive medium and one detection site. The potential in this case can be calculated by

$$\phi = \frac{1}{4\pi\sigma}\left(\frac{I_1}{r_1} + \frac{I_2}{r_2} + \frac{I_3}{r_3} + \frac{I_4}{r_4}\right) \tag{2.12}$$

Moreover, multiple voltage sensors can be defined at which the potentials (coupling weights) are independent and would be calculated instantaneously.

2.6 Insulated Boundaries as Reflectors

The potential in a conductive medium due to a point current source is proportional to the current magnitude and inversely proportional to the medium conductivity, as determined from Eq. 2.10. It is critical to have a wide range of potential measurement values and large magnitudes in order to distinguish output shapes and acquire better resolution. This can be done by either reducing the medium conductivity or

increasing the current input magnitudes. Reducing the medium conductivity may increase the chance of error in the contact between the pin source and the medium due to the porosity increase. Thus, increasing the current magnitude would be a suitable solution.

The input current source is driven by voltage controlled current circuits which requires relevant power magnitude. Therefore, power dissipation may be a concern, because low power is desired to be maintained. The insulated boundary is the best solution to increase current magnitude and decrease the conductive medium size as well. It is known that an insulated boundary, a Neumann boundary state, work as a mirror wall and the reflection of the medium is considered its extension.

For a cubic volume conductor, orthogonal planes on the X, Y, and Z axes bisect the space symmetrically. If each of these planes is defined as an insulator, the required volume of electrically conductive material is reduced without changing the current density or potential distribution in the medium. Moreover, not only is the potential magnitude multiplied and amplified in the cut medium but also a no constricting zone is assigned to the insulated boundary. The insulated boundary reflects the electrical current back to the conductive medium and so the potential increases, as shown in Fig. 2.12. Thus, when an input current source is positioned proximate to an insulated side, the potential magnitude range in a medium is doubled. Due to the symmetry of the bisected volume, the potential measurement at a corner of the conductive material cube is effectively unchanged from a potential measurement located at the center of a cubic volume that is eight times larger than the conductive cube. Three electrically insulated sides joined at a corner effectively increase the sensitivity of a voltage sensor positioned at the corner by a factor of eight. Therefore, the need to amplify the input signals is reduced and the electrically conductive material can occupy a smaller volume. Consequently, the EAC consumes less electrical energy during operation, while occupying less volume.

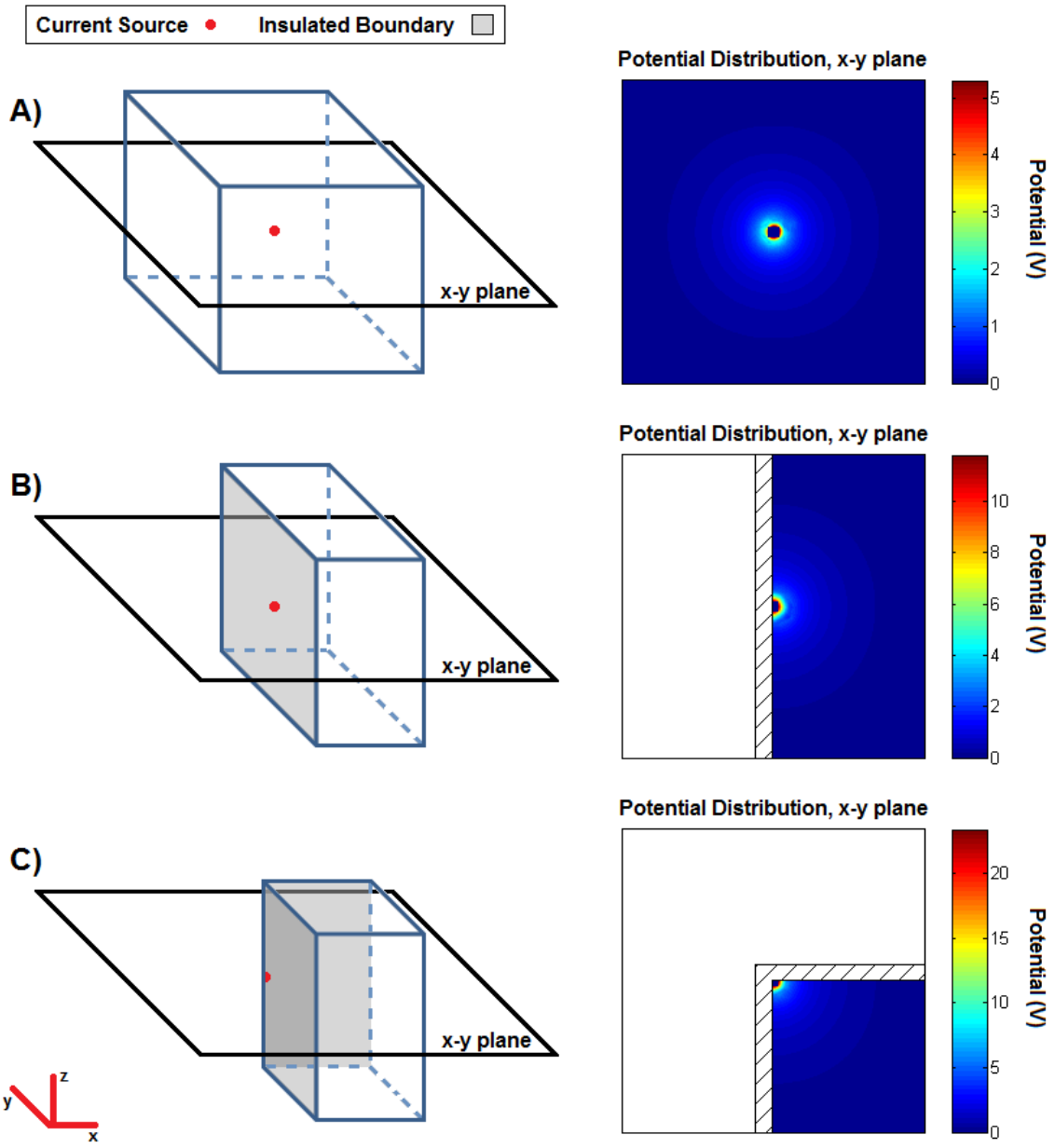

Fig. 2.12. Reflections of an electrical signal from electrically insulated sides of an electrically conductive material. (A) A centered current source in 1 cubic meter medium with grounded boundaries. (B) A current source proximate to an insulated boundary in $0.5 \times 1 \times 1$ m medium. (C) A current source proximate to two electrically insulated boundaries in $0.5 \times 0.5 \times 1$ m medium. The medium in the three cases is isotropic with conductivity of 1 S/m, where the current magnitude is 1 A. These results were simulated by COMSOL 3.5a.

2.7 Effect of the Shape of the Current Source

2.7.1 Point Source vs. Line Source

Shapes of current sources may affect the potential distribution in the volume conductor of the EAC. Thus, different shapes of current sources were considered and analyzed. Point current source is the simplest source configuration, in which current is emitted in all radial directions with the same current density. In practice, point sources do not exist because they have zero volume and zero surface area; however, spherical sources have the same current density characteristics as point sources. Line sources behave differently from point sources. They emit currents only in the radial direction normal to the line source, as shown in Fig. 2.13. They do not exist because they have zero volume and zero surface area; however, cylindrical sources have the same current density characteristics as line sources as they emit current normal to the cylinder surface.

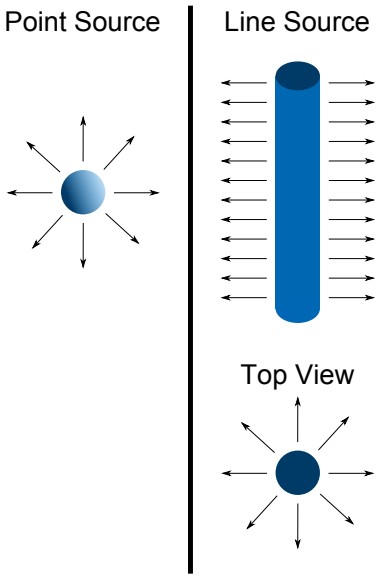

Fig. 2.13. A schematic of point current source vs. line current source. Point source emits current radially in all directions (left). Line current source emits current in radial directions normal to the line source (right).

Due to the difference in current densities and directions, the potential distribution is also different as shown in Fig. 2.14. In the point source case, equipotential (isopotential) lines are circular until they reach to the restricted zone where they become rounded rectangular. In contrast, in the line source case, equipotential (isopotential) lines are rounded rectangular in all planes that are perpendicular to the line source.

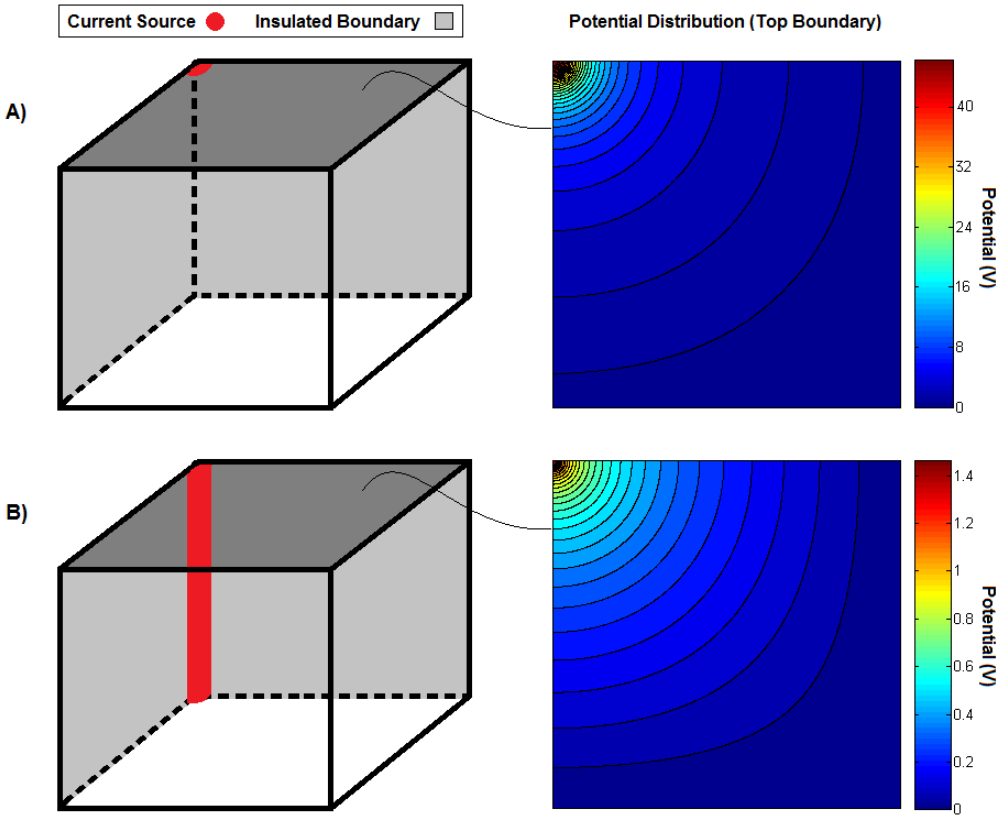

Fig. 2.14. Potential distribution as a result of a point current source vs. line current source. (A) Potential distribution at the top boundary plane that includes the current source when injecting current of 1 A with a point current source in an isotropic 1 cubic meter medium with conductivity of 1 S/m. (B) Potential distribution at the top boundary plane when injecting current of 1 A with a line source in the same conductive material characteristics as in (A).

2.7.2 The Disc Source

Spherical sources are not easy to design and manufacture. Disc sources, however, are easy to manufacture and commonly used in various applications. The analytical solution of the potential distribution as a result of a disc-shaped current source is not easy to obtain because of the difficulties in finding the current density and direction. The potential distribution is not the same in all directions as in the case of spherical source. The disc sources (electrode pins), however, would be placed adjacent to each other in the EAC, as shown in Fig. 2.15, so that the distribution in only the horizontal (xy) plane is the point of interest.

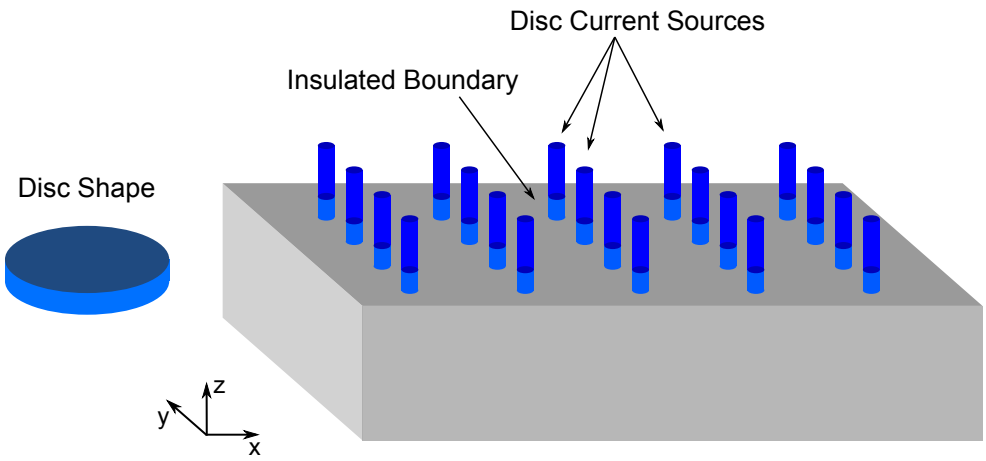

Fig. 2.15. Disc source orientation in the EAC conductive medium.

Using COMSOL 3.5a, potential distribution due to the disc source in the xy plane was determined and compared to the potential distribution due to the sphere source. The potential distributions appeared to be identical, as shown in Fig. 2.16. Therefore, disc sources can replace sphere sources in the EAC where all analysis done on the sphere source is valid for disc sources.

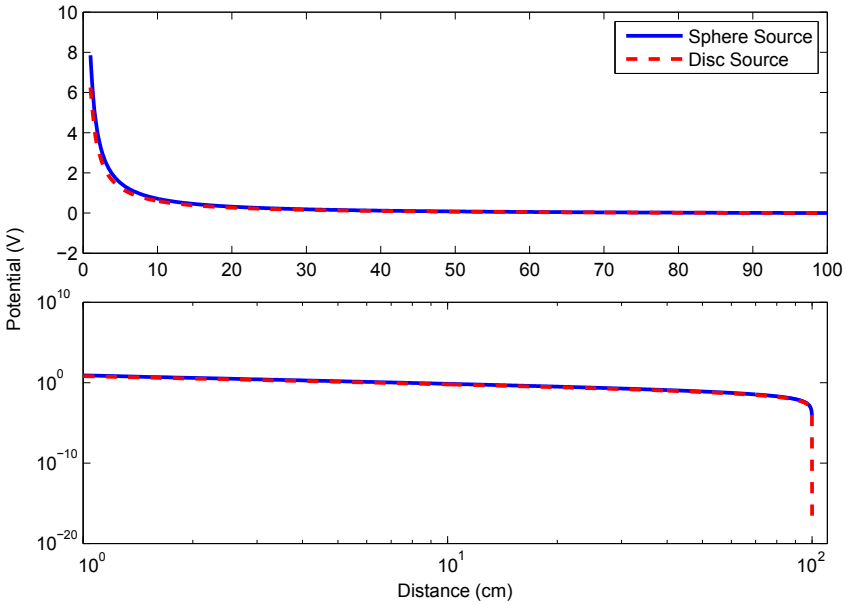

Fig. 2.16. A comparison between the potential distribution for a sphere and disc source using COMSOL 3.5a, where the source is at the center of an isotropic spherical medium with a radius of 1 m and conductivity of 1 S/m at grounded boundary state. In both cases, the current source magnitude was 1 A.

3. EAC OPERATING ON FUNCTIONS OF TIME

3.1 Time Domain and Linear Filters

The EAC not only works in a spatial manner to perform mathematical operations as explained above, but it can also work in a temporal manner to perform functions such as signal filtering and solving linear time-invariant systems if a means can be devised to represent time on the manifold. In other words, functions of time can be processed if one of the spatial dimensions in the EAC medium is mapped to time. Sample-and-hold circuit is used to allow practical mapping of continuous time to space. It samples the analog input signal to quantized time intervals [38]. Calculations are then performed on the sampled-time signal to implement a tapped analog delay line filter that solves arbitrary FIR filter. The EAC takes on the appearance of a tapped delay line filter, but where the weights are defined by the sensitivity weights of the sources.

3.2 Finite Impulse Response (FIR) and Infinite Impulse Response (IIR) Filters

FIR filters, also called moving average (MA) filters, are always stable because they only perform calculations on present and finite delayed samples of the input [39]. The output of the FIR filter is a weighted sum of the present and a finite number of previous input values solving the equation

$$y(n) = \sum_{i=0}^{M} b_i x(n-i) \tag{3.1}$$

where $y(n)$ is the output filtered signal at time n, b_i are a set of M weight factors for an order M filter, and $x(n-i)$ represents the time signal $x(n)$ at the present

time and for each $1 \cdots M$ discrete time increments in the past. Filter weights, b_i, are critical characteristic that discriminate an FIR filter from another. These weights are inversely proportional to the distance from the sources taps to the detection point (output).

IIR filters, however, are not necessarily stable because they perform calculations on the output delayed samples (feedback) [39]. These filters are also called autoregressive (AR) filters. The output of the IIR filter can be calculated by the equation

$$y(n) = \sum_{j=1}^{N} -a_j y(n-j) \tag{3.2}$$

where $y(n)$ is the output filtered signal at time n, a_j are a set of N weight values, filter coefficients, for the output delayed samples $y(n-j)$, where N is the filter order.

IIR filters are usually replaced by a combination of FIR and IIR filters where the computations include time-delayed inputs and outputs which are called FIR-IIR or autoregressive moving average filters (ARMA). The performed equation of the FIR-IIR filter is as follows

$$y(n) = \sum_{i=0}^{M} b_i x(n-i) + \sum_{j=1}^{N} -a_j y(n-j) \tag{3.3}$$

where $y(n)$ is the output filtered signal at time n, b_i are a set of M weight values, feedforward filter coefficients, for the input present and delayed samples $x(n-i)$, where M is feedforward filter order, a_j are a set of N weight values, feedback filter coefficients, for the output delayed samples $y(n-j)$, where N is the feedback filter order. M and N are usually the same where they denote the filter order. Fig. 3.2 shows a block diagram of the FIR-IIR filter. The EAC can perform these calculations by recursion which can be presented in one sheet where an output of a sheet is wired to an input on the same sheet. This would allow implementing infinite impulse response (IIR) filters where the output is accumulated to allow infinite memory storage.

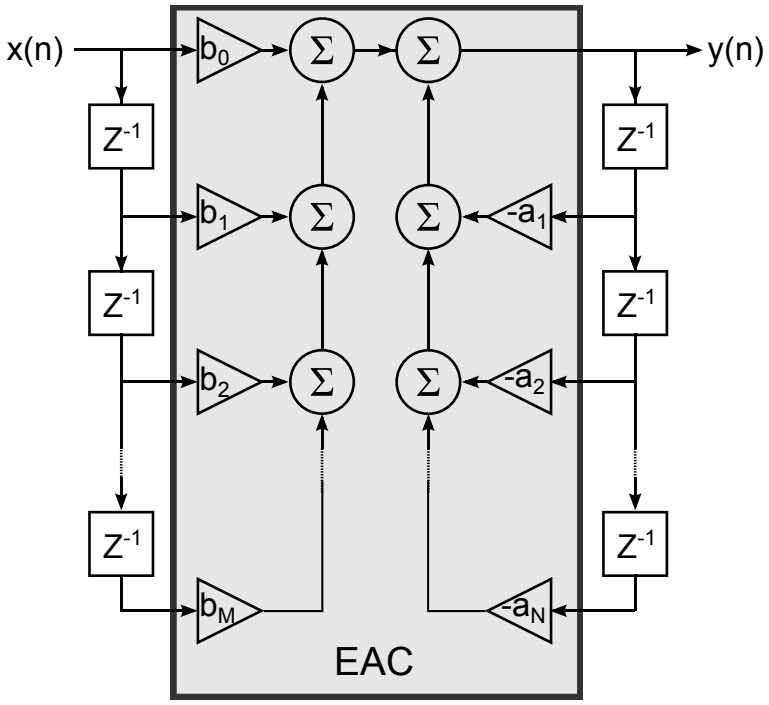

Fig. 3.1. A block diagram of FIR-IIR and calculations done by the EAC.

3.3 Prior Art of Analog FIR Filters

The tapped analog delay line (TAD) filter is a means to implement filtering or calculations of solutions to ordinary differential equations using analog circuits. Real-time filtering with TAD was first introduced by N. Wiener during the 1940s [40] and successfully applied in various applications such as automatic equalization for digital communication [41]. TAD-N is a device that stores the N most recent input signal samples so that there are N independent delay lines, which are loaded and clocked simultaneously [42]. These taps are then multiplied by the corresponding weights of the desired FIR filter. Physically, this is done by wiring each of the TAD-N outputs by a resistor with resistance values proportional to the reciprocal of the FIR filter weight. An operational amplifier is then implemented to sum all the outputs to give the filtered output.

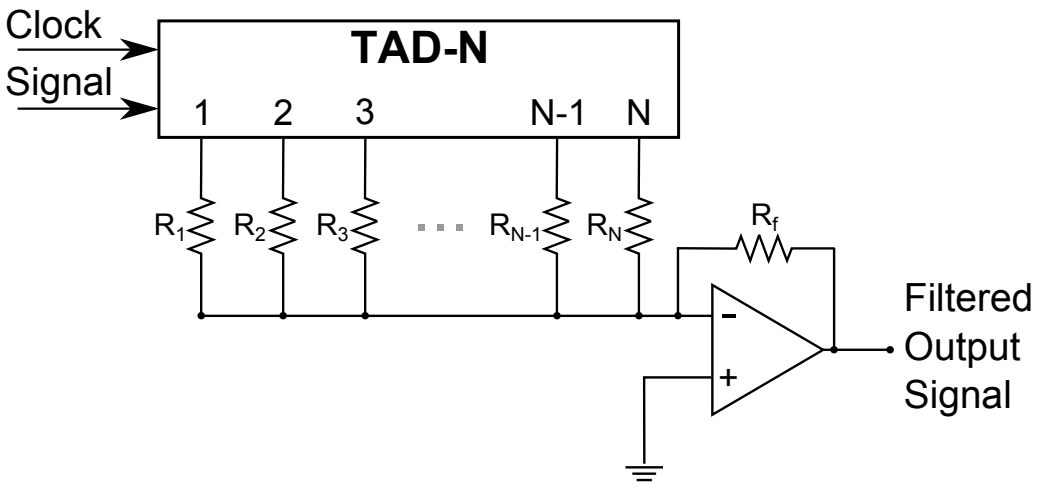

Fig. 3.2. A schematic of a tapped analog delay line (TAD) transversal filter. TAD-N is used to store the N most recent input signal samples and then the weighted sum of these weights are calculated with a summing amplifier.

In the resistance mode, the EAC works as a multiplier and an integrator. As discussed above, the EAC medium works as a series of resistors in three-dimensions and a summer as well. Therefore, the outputs of the TAD can be simply wired to different locations on the EAC where the distances between the TAD outputs and the detection point are inversely proportional to the FIR filter weights. The voltage value of the detection point represents the filtered signal. As such, the EAC can be configured as a discrete-time finite impulse response (FIR) filter using a tapped delay line transversal filter. Architecturally, the complementary configuration for recursion could be applied to the EAC to a discrete-time infinite impulse response (IIR) filter. The combination of the FIR-IIR, thus would enable the EAC to calculate solutions to arbitrary N^{th} order transfer functions.

3.4 The Reciprocity Theorem

We observed that the resistance mode EAC works identically to how an electrode picks up potentials from a myelinated nerve fiber. The nodes of Ranvier on the myelinated nerve fibers are modeled as discrete current sources. The current source waveform jumps from one node to another, where the traveling wavefront and waveform is the summed action current from the channels at each node. They travel with a time delay, which is related to the conduction velocity of the SFAP, as it travels down the nerve fiber [5] [43]. This looks a lot like what the EAC does. Reciprocity theorem was used to simplify the calculations in order to analyze how the electrode picks up activity from myelinated nerves [5]. The weight space remains constant for every electrode pickup point. So, the extracellular SFAPs from arbitrary fibers can be simulated as long as the path of the fiber and its conduction velocity is known. This function turns out to be identical to that of the EAC using a tapped delay line. So, this theorem was adapted to analyze how to place sources and sinks in the conductive medium to generate the appropriate weights for the desired filter.

The reciprocity theorem is the bases of the lead field theory in a volume conductor to evaluate measured signals in terms of their sources [36]. The principle of reciprocity was first introduced by Hermann von Helmholtz over 150 years ago to solve various problems in bioelectromagnetism [44]. The theorem demonstrates that the source and measurement locations can be swapped without any change in the signal. This means that for a measurement site and specific pattern of current sources locations in a conductive medium is the same if the detection site becomes a current source and current sources become detection points. This is a very important concept for bioelectromagnetic problems. This theorem was used to analyze filter characteristics, as explained later.

3.4.1 Time-Space Relationship

The spatial configuration of the input pins around a given potential detection site affects the operation of the FIR filter. The distance between the input pins from each of the input taps, however, does not affect the operation of the filter. Previous work showed the link between the spatial frequency domain and time frequency domain relationship [5] [43] [45] . The function for the filter can be represented in a time-space relationship based upon the reciprocity theorem with the following equation

$$V(j\omega) = (\frac{1}{f_s})W(\frac{j\omega}{f_s})I(j\omega) \tag{3.4}$$

Where $V(j\omega)$ is a frequency-domain representation of the output signal, f_s is the sampling frequency of the input signal, $W(j\omega)$ is the frequency-domain representation of the weighting function that is inversely linearly scaled by the inverse of the sampling rate, and $I(j\omega)$ is the frequency-domain representation of the input current for each tap in the filter. The weighting function W, is influenced by both the sampling rate f_s, and the locations of the inputs relative to the voltage sensor. This equation was originally found for a similar situation to the Bessel filter architectural design on the EAC. It was found for a single fiber action potential (SFAP) traveling through a myelinated nerve fiber in a conductive medium.

3.5 The Bessel Filter

Like an electrode picking up a traveling point source in the tissue volume conductor, the filter function of a uniform conductive medium is a Bessel filter whose corner frequency depends upon the speed of the point source and its distance from the detection point. A Bessel filter is an example of FIR filters that is linear with a reasonably constant group delay [46]. In an isotropic medium with Neumann grounded boundary state and conductivity of σ, an array of $N+1$ sources is initially defined, where $N+1$ is the filter order. These sources are distributed evenly-spaced in a straight line with a perpendicular d distance away from the potential detection point, as shown in Fig.

3.3. The input signal, $x(n)$, is to be sampled by an analog sample-and-hold circuit with a sampling rate of f_s. The sample-and-hold buffers generate N of incrementally time delayed versions of the input signal. For example, when the EAC is configured as a filter with $N+1$ taps, the EAC uses a total of N sample-and-hold buffers, one for each of the N delayed signals.

Nominally, the time-delayed sources distribute to implement a low pass filter function which is dependent on the distance from the source and the voltage sensor d and the sampling frequency f_s. Filter characteristics such as cutoff frequency and phase can be tuned by many factors such as medium conductivity, sampling frequency, and space sampling interval. On one hand, as the detection point gets closer to the sources array (x-direction), the cutoff frequency of the filter gets higher while the phase remains the same. On the other hand, as the detection point is moved in parallel to the sources array (y-direction) towards $x(n-N)$ tap, the phase gets slightly delayed. Thus, the system is considered non-causal with only a group time delay.

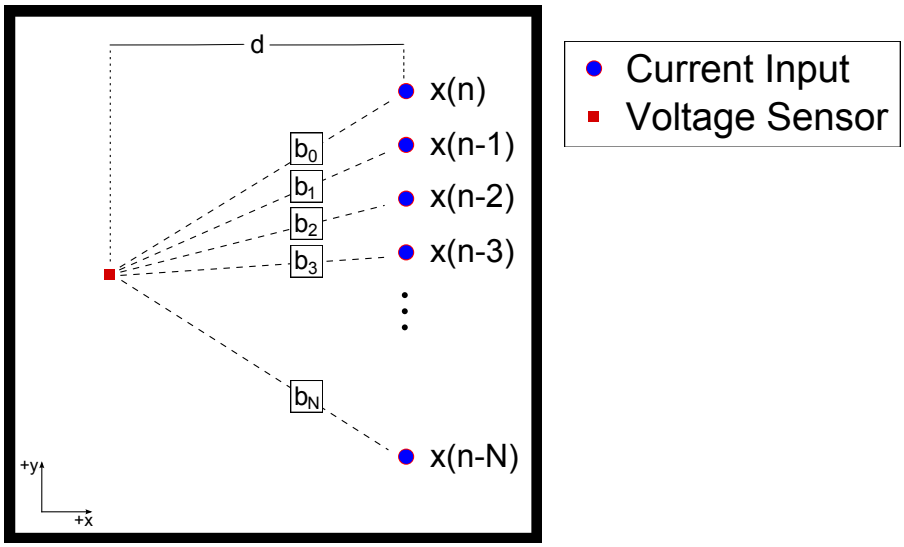

Fig. 3.3. A schematic of Bessel filter configuration on the EAC. $x(n)$ is the input signal and b_i are the filter weights which are inversely proportional to the distance between the sources and the voltage sensor.

3.5.1 Analytical Solution of the Bessel Filter

The Bessel filter function can be derived analytically. The function is equivalent to the Fourier Transform of the weighting function, which is inversely proportional to the distance between the sources and the detection point. Based on the reciprocity theorem the weighting function can be determined by injecting current through the detection site and measuring the potential at the current source sites. Then, the Fast Fourier Transform of the weighting function gives the characteristics of the filter.

The charge potential distribution of a point current source in a homogeneous and isotropic conductive medium can be determined by Eq. 2.10, where I is the current source magnitude, σ is the conductivity value of the medium, and $r = \sqrt{x^2 + y^2 + z^2}$ where the current source is located at (x, y, z) while the field point is at the origin. At a horizontal 2D plane where $z = 0$, (xy plane), the potential distribution can be estimated by the equation

$$\phi = \frac{I}{4\pi\sigma\sqrt{(x^2 + y^2}} \tag{3.5}$$

For an array of sources that lie on a straight line that is at a perpendicular d distance from the current source, shown in Fig. 3.5, the potential distribution is as follows

$$\phi = \frac{I}{4\pi\sigma\sqrt{(d^2 + y^2}} \tag{3.6}$$

This potential distribution represents the weighting function of the filter. Therefore, the spatial frequency response of the filter can be determined by applying the Fourier Transform of the weights

$$\phi(\omega) = \int_{-\infty}^{\infty} \frac{I}{4\pi\sigma\sqrt{(d^2 + y^2}} e^{-2\pi i\omega y} d\omega \tag{3.7}$$

where ω is the spatial frequency.

Using MATLAB 2009a (The MathWorks, Inc. Natick, MA), for symbolic integration, the filter function becomes

$$\phi(\omega) = \frac{Ibesselk(0, |\omega|d)}{2\pi\sigma} \tag{3.8}$$

where $besselk(n, m)$ is the n^{th} order modified Bessel function of the second type of m. Fig. 3.5 shows the low-pass filter behavior for a various string of sources away from the detection point as a function of the spatial frequency. The cutoff frequency of the filter decreases as the distance between the source array and the voltage sensor increases.

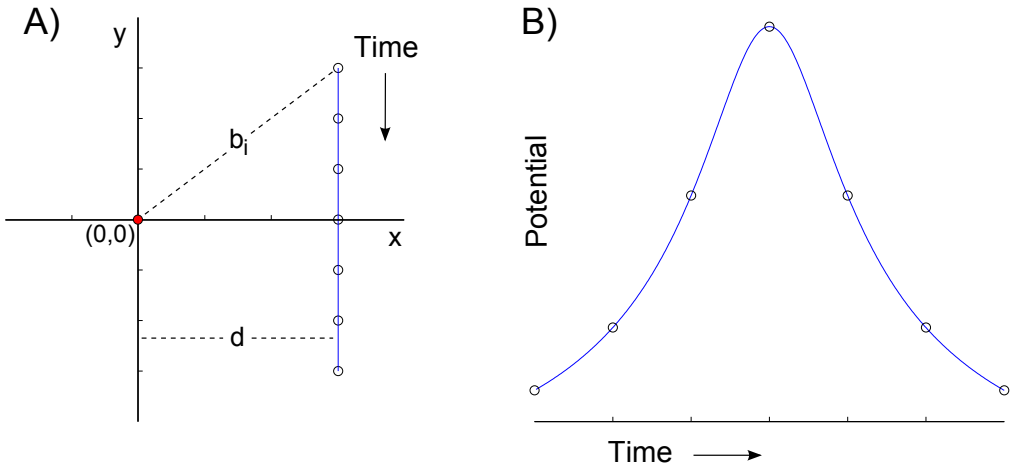

Fig. 3.4. Bessel filter analytical solution procedure. (A) shows the current sources array in a straight line at a perpendicular distance d away from the detection point. (B) shows the filter weighting function which is inversely proportional to the distance between the sources and the detection point.

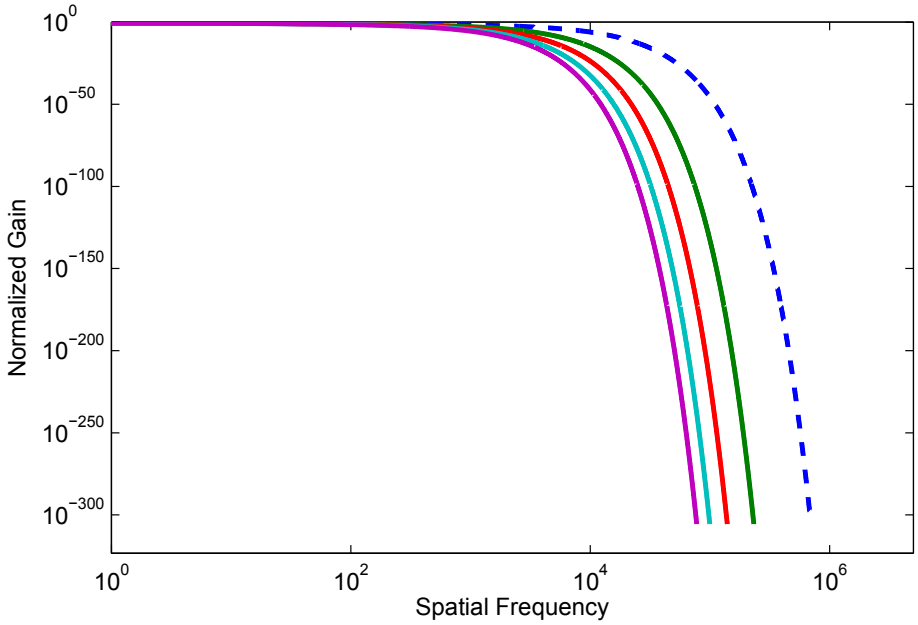

Fig. 3.5. A representation of the analytical solution of the filter function at different distances from the detection point where the blue-dashed curve is the closest.

3.5.2 Bessel Filter with Different Shapes of Sources

As discussed above, the shapes of the current sources may induce different potential distribution in the medium. Subsequently, the weighing functions of the FIR filter due to different sources shapes are different. Therefore, the Bessel filter behavior was analyzed with three most common sources shapes: spherical, cylindrical, and disc. The filter gains are shown in Fig. 3.6. Spherical and disc sources show a wide range of cutoff frequencies with different distances that match the driven Bessel filter analytical solution. However, cut-off frequencies range for the Bessel filter due to cylindrical sources is narrow. Since disc sources are easy to manufacture, they are preferred in Bessel and FIR filter implementation in the EAC.

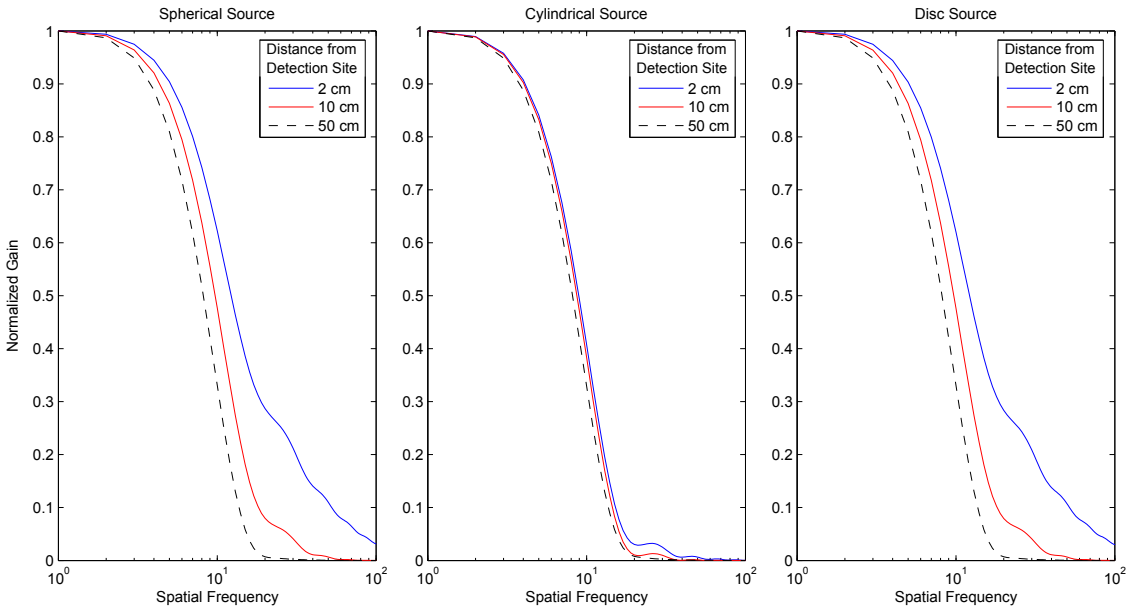

Fig. 3.6. The filter gain with different sources shapes for various distances between the sources and the detection point.

3.5.3 Filtering Demonstration

To demonstrate the Bessel filter effect, a two-dimensional arrangement of input pins and voltage sensors that are configured to act as a Bessel filter, which is one type of FIR filter. As shown in Fig. 3.7, a total of eight (8) input pins receive the input signal which is the recent and seven (7) time-delayed current values. In a cubic electrically conductive medium, two vertically adjacent boundaries were insulated where the others were grounded. The most recent input sample of the signal $x(n)$ is supplied to an input pin proximate to the center of one of the insulated sides of the conductive medium. The eight input pins are selected in a linear arrangement with the time delay increasing by one time increment for each successive input pin. Three voltage sensors were introduced where each of them is located at a constant distance from the line of input pins along the $x-$axis. Each of the voltage sensors detects a potential corresponding to the Bessel filtered output signal of the input signal $x(n)$.

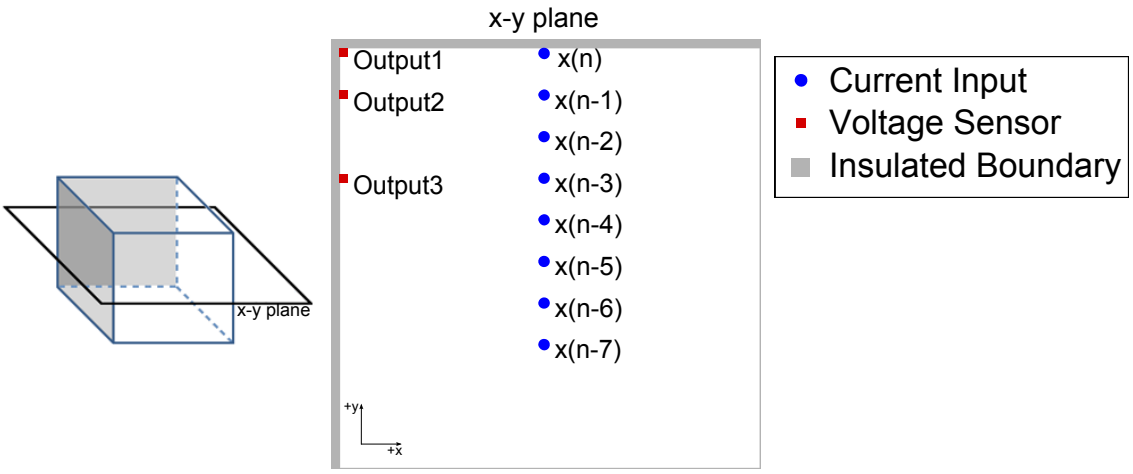

Fig. 3.7. A schematic shows the Bessel filter configuration for filtering demonstration. Family of filtered signals with different characteristics was observed.

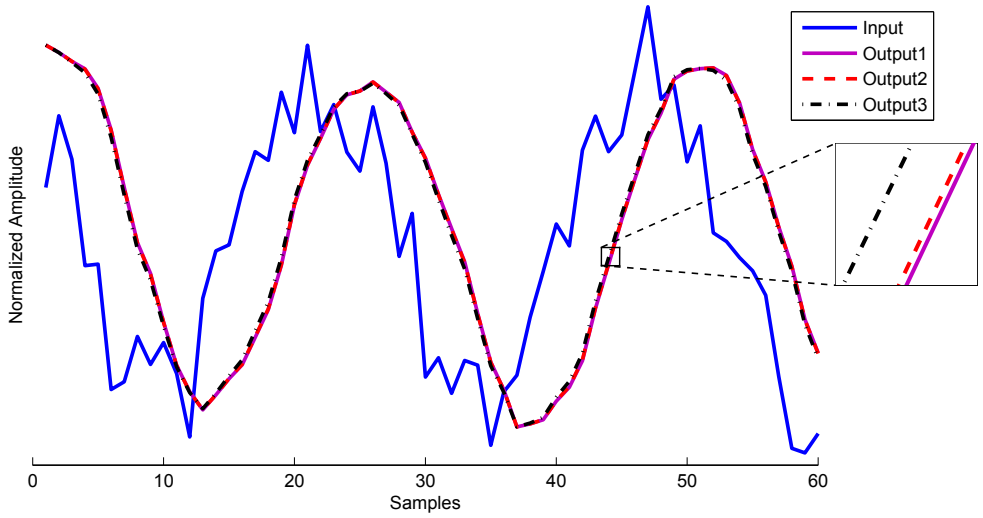

Fig. 3.8. The filtering effect of a 60 sample sinusoidal current input with white noise added. Voltage sensors at different sites show low pass filtered signals with a group delay and slightly more delays as the detection site gets closer to $x(n)$ tap.

The distribution of the voltage sensors from the center of the linear arrangement of input pins generates a slight time-offset in the detected output signals $y(n)$. Thus, the voltage sensors detect a family of Bessel filtered signals in parallel. As shown in Fig. 3.8, voltage sensors (Output1, Output2, and Output3) detect the filtered signal with the smallest amount of time-offset in addition to the group delay compared to the original input signal $x(n)$. Consequently, the EAC can generate multiple filtered output signals with different characteristics in parallel.

3.6 Implementing Arbitrary FIR Filter with the EAC

Any arbitrary FIR filter can be implemented on the EAC by allocating the appropriate locations of the sources where their distances to the potential detection point are inversely proportional to the filter weights. A grid pattern of pins would be initially placed in the conductive medium to accept different weight-distances. The input pins would be spaced apart equidistant from each other similarly to vertices in a series of stacked cubes. But in order to find the exact locations of the sources for accurate weight values, infinite resolution of input pins must be implemented. In reality, this is not possible; however, large density of grid pins is preferred.

In alternative embodiments, the input pins can be arranged differently and not necessarily spaced apart equally. For example, in a conductive medium with two adjacent insulated boundaries in addition to the top and bottom boundaries, the pins could be arranged in a plurality of radial lines extending outward from the voltage sensors, as shown in Fig. 3.9. The input pins would be arranged in a denser configuration near the voltage sensors, and spaced at increasingly greater intervals as the distance from the voltage sensor increases. The arrangements of the input pins and the voltage sensor are arranged in a two-dimensional configuration on the conductive medium instead of the three-dimensional configuration. This architectural design represents an FIR filter where the number of radial lines represents the filter order, the number of pins in each radial line represents the bit resolution of the filter

weight values that can be implemented on the EAC, and the center of the circular pins is the potential detection site which represents the output of the FIR filter $y(n)$.

The pins in the radial line carry the same input current; however, each one of them is controlled by a binary gate, as shown in Fig. 3.10. This is similar to an R-2R Ladder circuit which is a simple circuit that consists of only resistors to perform digital to analog conversion. Every weight value can be precisely adjusted by selecting the appropriate combination from the array of the eight taps. These combinations of values are summed be the EAC to represent an 8-bit value of the weight. Since the potential distribution in a conductive medium due to a point current source follows a rational function, the distance between the 8 radial pins must be doubled as getting further from the detection point in order to match the power-of-two expansion where each pin implies half the amplitude of the previous one to allow 2^8 possible weight values. Thus, the displayed 8 pins can implement an 8-bit resolution of the filter weight values. A greater number of input pins at varying distances from the voltage sensor provide a higher resolution for selecting different weight values to improve the performance of the FIR filter.

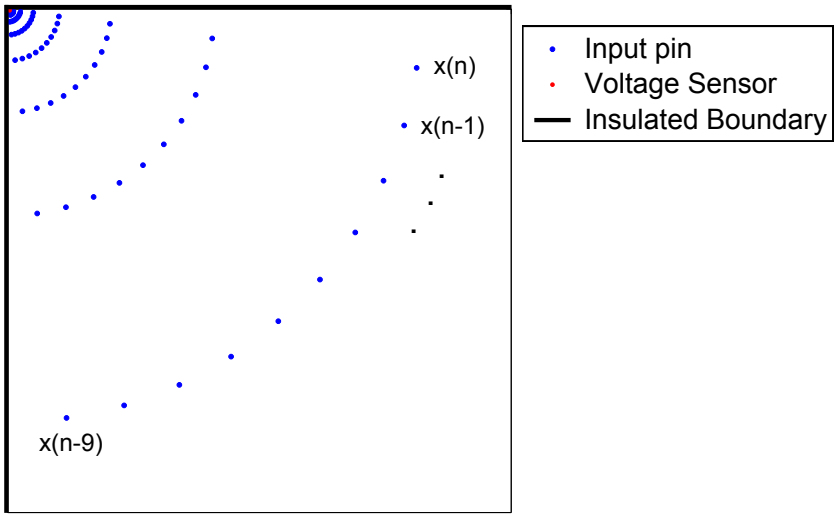

Fig. 3.9. A schematic of an FIR filter configuration to implement an arbitrary 8-bit weight resolution, 10^{th} order FIR filter.

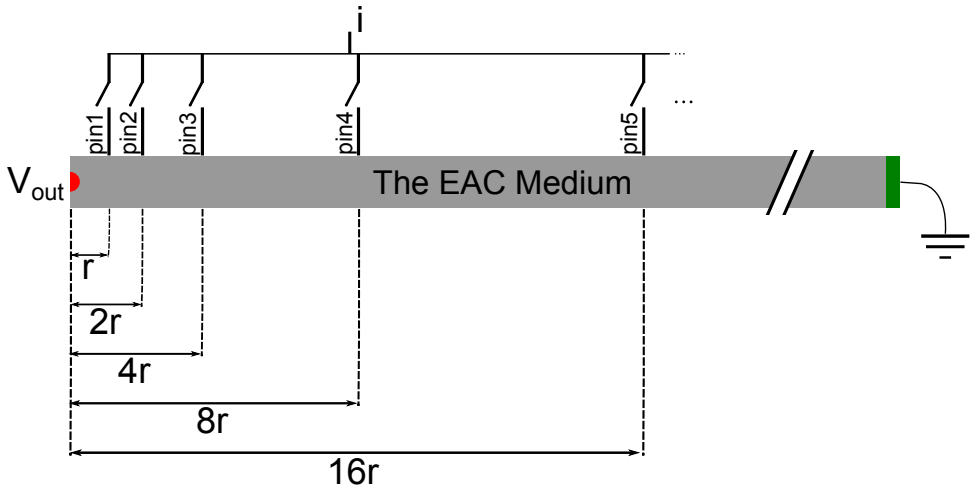

Fig. 3.10. A schematic of one input source shows the n-bit digital to analog conversion with a binary gate for each pin. I_0 is the input current and r is the distance between pin1 and the detection point V_{out}.

3.7 Filter Weights

As described above, the weight value for each input tap varies with the distance that separates the input pin and corresponding voltage sensor. The weight value is always positive since it is inversely proportional to distance between the input pin and the voltage sensor in the electrically conductive material. We can, however, take advantage of multiple detection points and take the differential voltage measurement to consider negative weight values. To consider a negative weight value, the EAC measures two different charge potentials V_1 and V_2 using two of the voltage sensors and a single input pin corresponding to the tap with the negative weight value. For an input source that is at r_1 and r_2 distance from the detection points V_1 and V_2 respectively, as shown in Fig. 3.11, if r_1 is larger than r_2, the electrical coupling weights between the source and the detection points become $1/r_1$ and $1/r_2$ respectively, where $1/r_1$ is smaller than $1/r_2$. Thus, the differential measurement $V_1 - V_2$ is negative. Therefore, positive or negative filter weights can be implemented with the

EAC using differential measurement of two voltages at two detection sites where the weighting function W follows the equation

$$W(i) = k\Big(\frac{1}{r_1(i)} - \frac{1}{r_2(i)}\Big), \quad i = 1 \cdots N \tag{3.9}$$

where i is the source tap number in N sources, $r_1(i)$ and $r_2(i)$ are the distances from the source i and the voltage sensors V_1 and V_2 respectively, and k is a scaling factor that is related to the conductivity of the sheet and the reflections due to insulated boundaries in the medium.

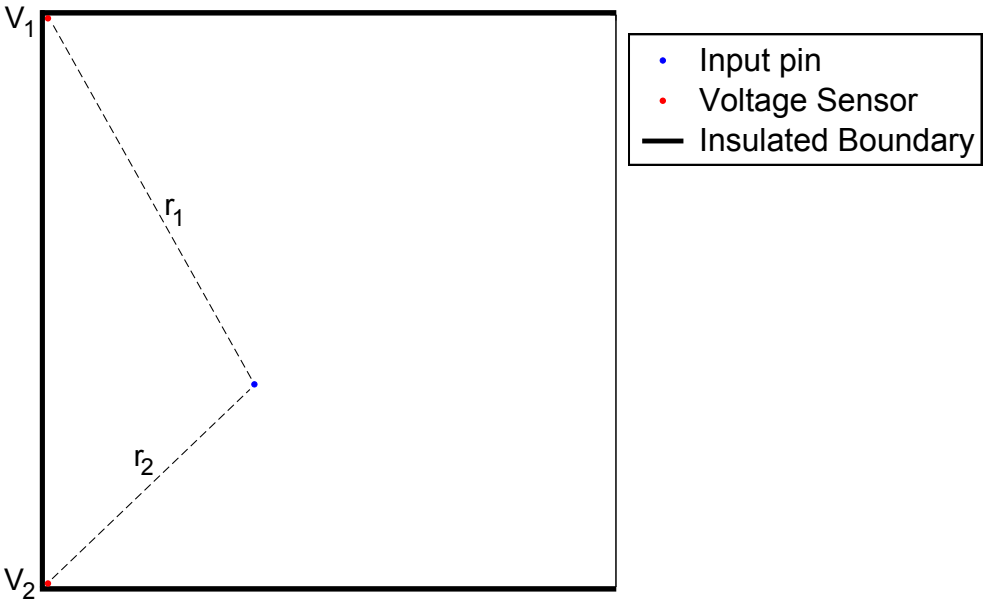

Fig. 3.11. A schematic of differential measurement procedure in the EAC. Differential measurement implies positive and negative weight values as desired.

The differential measurement response value is generally expressed in terms of variables that are dependent upon time and position within the field [27]. Therefore, it is defined as a dependent variable that is conveniently identified as a across variable. The across variable relates the condition at one point and relates it to another arbitrary reference point within the field. The measurements at two separated

points is simultaneously recorded within the field and their difference is defined as the differential potential difference or differential measurement. On the other hand, the through variable is the same everywhere within the element and does not require specifying two measurement points. Mathematically speaking, the across variable is the difference between two scalar potentials, while the through variable is a vector [27].

Using MATLAB 2009a, a computational algorithm was created to find random x and y coordinates that correspond to the weighting function and satisfy Eq. 3.9. For a weight value of b_0, a random distance r_1 is generated and r_2 is then calculated by Eq. 3.9. Using the law of sines and cosines given the dimensions of the medium, x and y coordinate pair referenced to V_2 sensor pin is calculated. This process is repeated for all the weight values of the weighting function.

3.8 Family of Solutions

The EAC is a radical departure from the general-purpose digital computer and derives its computational power by taking advantage of the intrinsic solutions to partial differential equations represented by the creation of an analog voltage manifold in space. Unlike current conventional digital signal processing or analog computing, which sequentially solves one differential equation at a time, the EAC's voltage manifold forms to present families of solutions. For example, if a line of sources was considered for inputs in a regular grid EAC, as shown in Fig. 3.12, a family of detection points can be defined at which they represent Bessel filtered signals with different filter characteristics. Thus, the EAC is not only orders of magnitude faster, but it also provides richer processed information than current computing techniques.

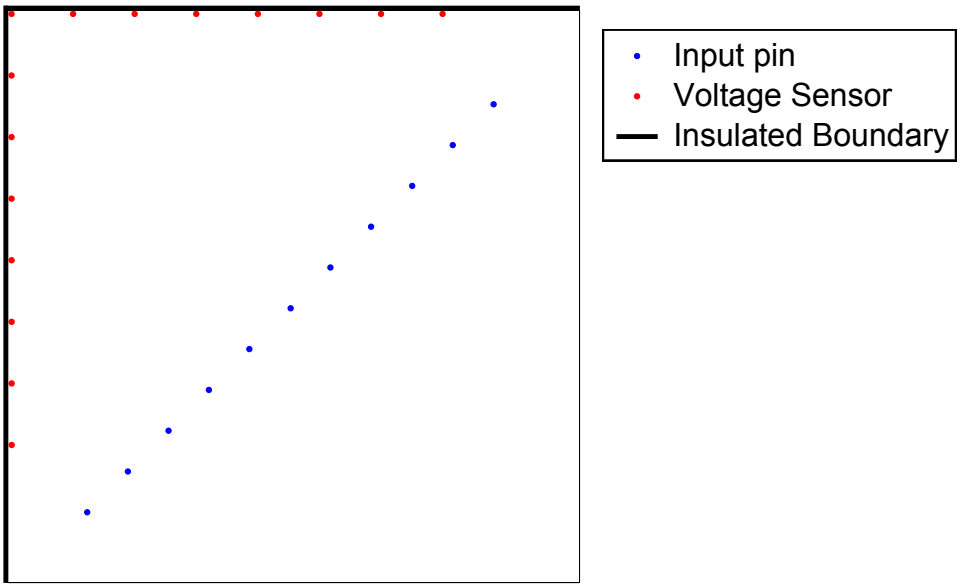

Fig. 3.12. Family of solutions can be detected simultaneously. Each voltage sensor represents a filtered signal with different filter characteristics.

3.9 Effect of Medium Thickness

The analytical solution of the Bessel filter function implemented on the EAC is under the assumption that the medium is of infinite extent. Therefore, large cubic electrical conductive medium gives a good approximation of potential distribution of the analytical solution. Less thickness with insulated boundaries, however, multiplies potential in the medium due to the reflection that is caused by the insulated boundaries. As the thickness of the medium gets lower, as more reflections occur. Consequently, different filter characteristics are achieved. To analyze the difference in filter characteristics with different medium depths, a centric point current source of 1 A was injected in different isotropic media with top and bottom insulated boundaries and conductivity of 1 S/m with depths of 1, 0.5, 0.25, and 0.1 m, where the other dimensions were kept fixed to 1×1 m. Then, the Fast Fourier Transforms of the potential at midline of xy plane (filter weights) that includes the current source

was calculated to give the filter gain characteristics, as shown in Fig. 3.13. It was found that the spatial cutoff frequency value of the filter increases as the thickness decreases.

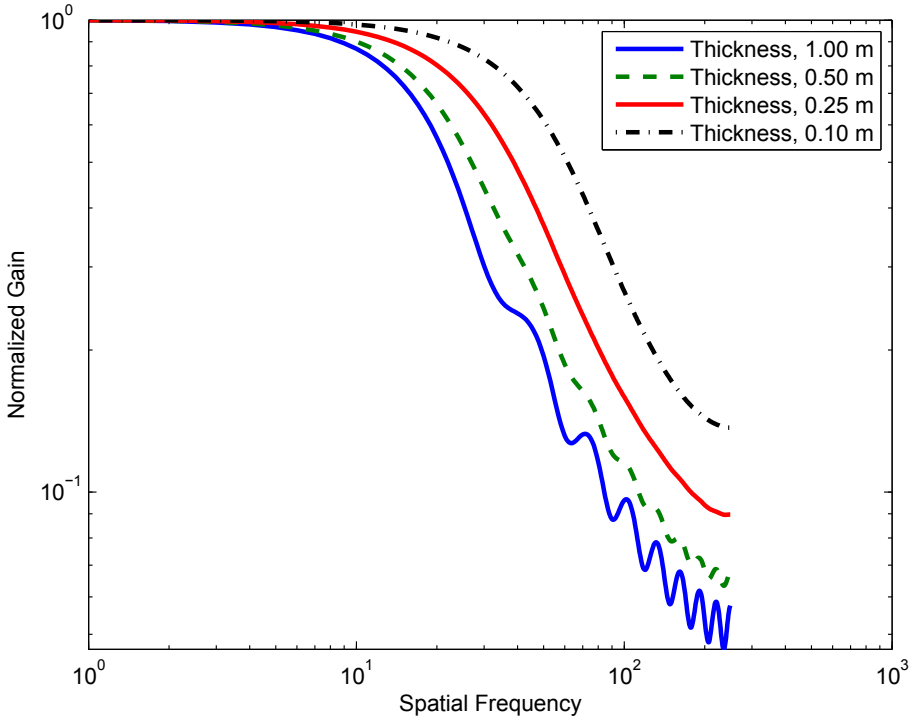

Fig. 3.13. Filters gain of Bessel filters implemented with different dimensions of the electrically conductive material in the EAC as a function of spatial frequency.

3.9.1 Compressing the Medium

In an alternative configuration, the electrically conductive material is formed with non-uniform dimensions. For example, the height of the electrically conductive material can be less than the length and the width of the electrically conductive material to reduce the physical dimensions of the EAC. It's desired to compress the medium and still have a compressed version of the same potential distribution so that it can

be designed as a small chip. When the dimensions of the electrically conductive material are non-regular or nonuniform, the electrically conductive material can be formed with anisotropic electrical conductivity instead of the isotropic conductivity for a cubic shape. For example, when the height (Z), or thickness, of the electrically conductive material is changed by a factor of t with reference to the width (X) and length (Y) of the material, then the electrically conductive material has three conductivity values σ_x, σ_y, and σ_z for each of the X, Y, and Z axes, respectively. The total conductivity matrix is defined with the following equation

$$\sigma = \begin{bmatrix} \sigma_X & 0 & 0 \\ 0 & \sigma_Y & 0 \\ 0 & 0 & \sigma_Z \end{bmatrix} \rightarrow \begin{bmatrix} \sigma_x/t & 0 & 0 \\ 0 & \sigma_y/t & 0 \\ 0 & 0 & t\sigma_z \end{bmatrix} \tag{3.10}$$

Fig. 3.14 shows COMSOL 3.5a simulations for three different medium thicknesses (1, 0.5, and 0.2 m) where the conductivity matrix was adjusted using Eq. 3.10. The potential distributions in the three media were the same, which shows the ability to reduce the EAC medium thickness and still get the same potential distribution by adjusting the medium conductivity.

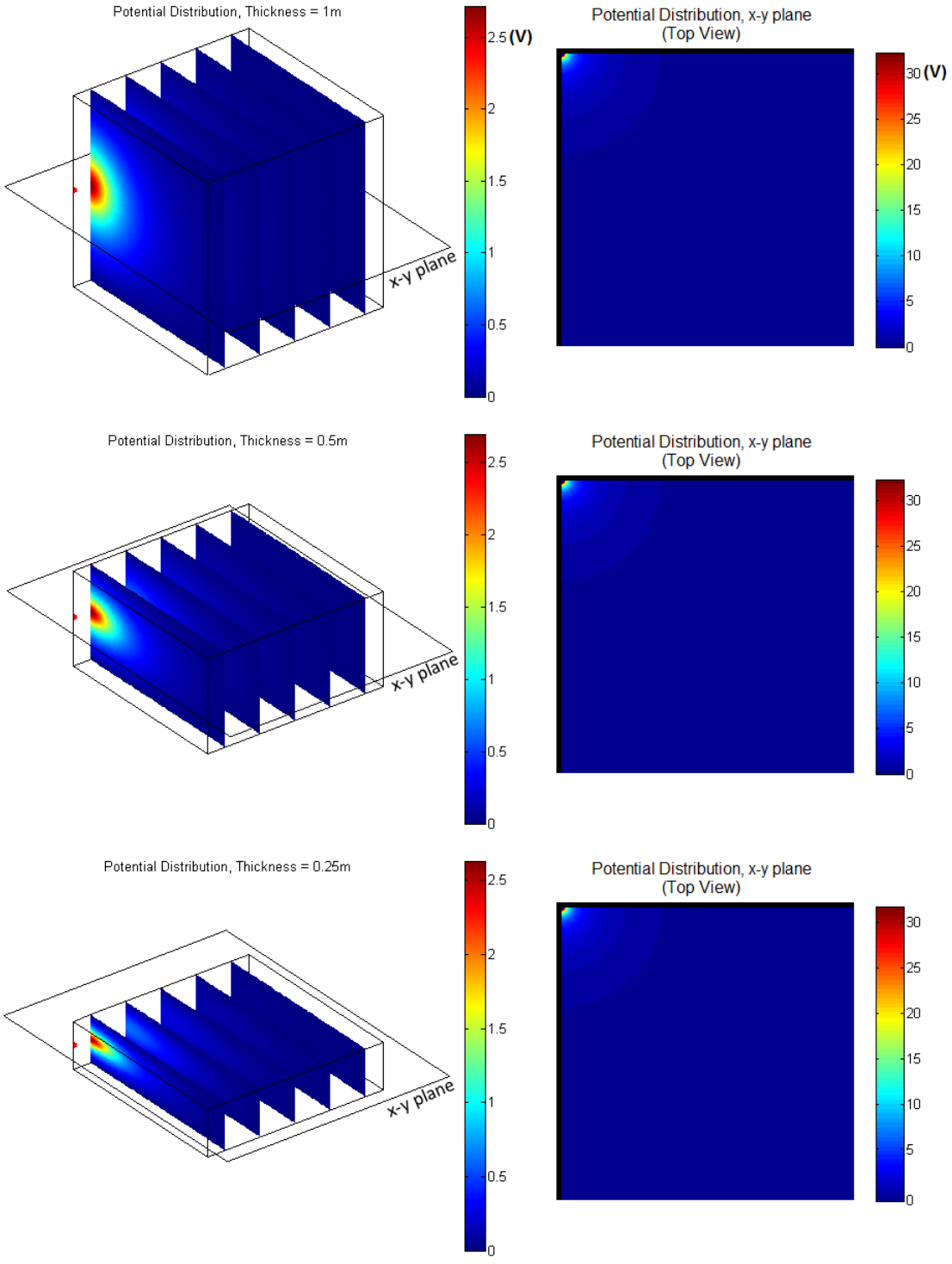

Fig. 3.14. A diagram of various dimensions and corresponding charge potential distributions of an electrically conductive material with different conductivity matrices. A current source of 1 A is placed in the mid intersection point of two insulated boundaries where the rest of the boundaries were grounded.

3.10 Arbitrary FIR-IIR Filter with the EAC

In contrast of finite impulse response (FIR) filters, infinite impulse response (IIR) filters are linear filters that have an infinite memory length where the filter acts upon the present and all past input samples. This is done by performing calculation using combination of finite delayed samples of the input and output, as shown in the FIR-IIR filter equation, Eq. 3.3.

For a 3^{rd} order low-pass Butterworth IIR filter with feedforward coefficients, b_i, of 0.0031, 0.0093, 0.0090, and 0.0031 and feedback coefficients, a_j, of -2.4222, 1.9969, and -0.5466, seven pin locations (x and y coordinates) in a conductive medium were found so that Eq. 3.9 is met in the differential measurement mode where the first four pins represent b_0, b_1, b_2, and b_3 and the other three pins represent $-a_1$, $-a_2$, and $-a_3$, as shown in Fig. 3.15. Then, the present and three prior delayed samples of the input stored in sample-and-hold buffers were assigned to the feedforward coefficients so that the performed equation calculated by the EAC of this part is the same for an FIR filter

$$y(n)_{feedforward} = \sum_{i=0}^{3} b_i x(n-i) = b_0 x(n) + b_1 x(n-1) + b_2 x(n-2) + b_3 x(n-3) \quad (3.11)$$

The most recent three output voltage samples were also stored in buffers so that they get recurred to the EAC medium to be involved in the next output calculations. These three most recent output voltage values were to be converted to currents by transconductance amplifiers and then injected to the feedback coefficient pins so that the performed equation is

$$y(n)_{feedback} = \sum_{j=1}^{3} -a_j y(n-j) = -a_1 y(n-1) - a_2 y(n-2) - a_3 y(n-3) \quad (3.12)$$

where

$$y(n) = y(n)_{feedforward} + y(n)_{feedback} \quad (3.13)$$

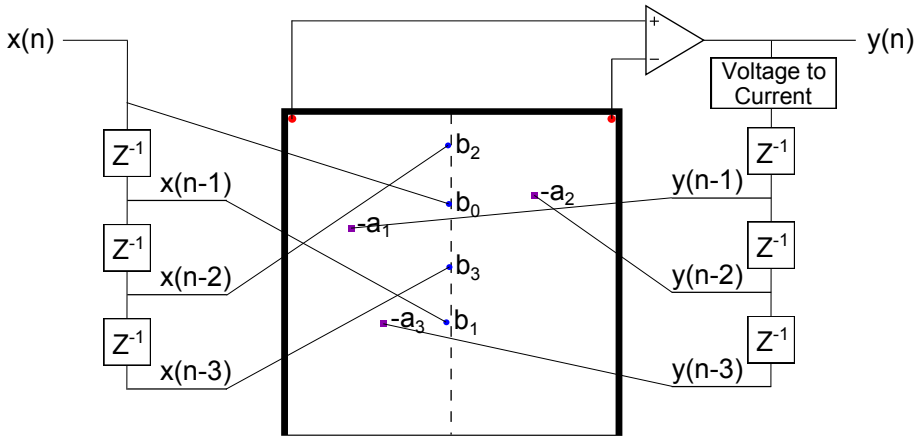

Fig. 3.15. A schematic of FIR-IIR low-pass Butterworth filter configuration implemented in the EAC.

One hundred samples of the impulse response of the system were determined by injecting an impulse function as an input signal $x(n)$ in the EAC configuration described above which was implemented in COMSOL 3.5a. As shown in Fig. 3.16, the impulse response of the EAC system was compared to the numeric impulse response of the same system determined by MATLAB 2009a and the error was calculated for every point to be less than 0.1%.

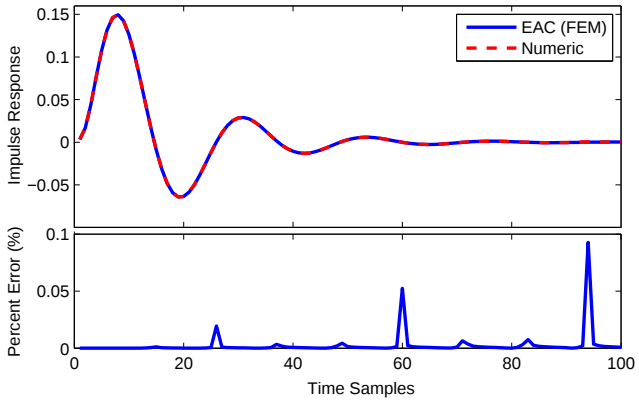

Fig. 3.16. Impulse response by the EAC vs. the numeric solution.

Furthermore, the Bode plot of the filter implemented by the EAC was determined and compared to the numeric Bode plot, as shown in Fig. 3.17. They were found to be virtually identical with little to no differences observed. This proves that an FIR-IIR filter can be implemented on the EAC. Using this method of configuration, any arbitrary linear transfer function can be implemented. The implementation is only practically limited by some factors such as the packing density of the sites and the number of sample-and-hold transconductance amps, and the bandwidth of the sample-and-hold electronics. For example, for an N^{th} order FIR, IIR, or a FIR-IIR filter, N contact pins on the EAC and sample-and-hold buffers ($2N$ for FIR-IIR) are required. The number of pins is limited by the size of the pins (diameter) and the dimensions of the conductive material. Moreover, sources and measurement points should be placed outside the restricted zone (10% from grounded boundaries) and relatively apart from each other. The order of the filter is also limited by the hardware of the EAC by the number of sample-and-hold buffers in both the input sample-and-hold circuit and the transconductance amps. The bandwidth of the sample-and-hold electronics may also cause some limitations of the speed of the EAC device.

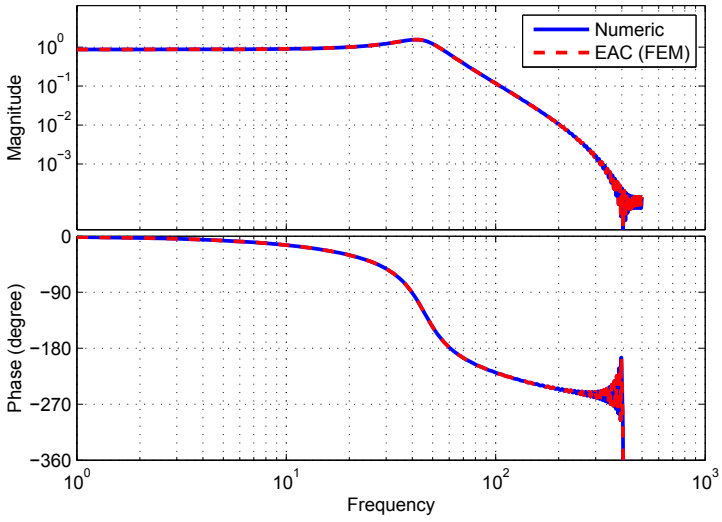

Fig. 3.17. Bode plot of the FIR-IIR filter by the EAC vs. the numeric solution.

4. NEURAL SIGNAL PROCESSING WITH THE EAC

4.1 Introduction

A practical application of neural signal processing is detecting and identifying single fiber action potential (SFAP) within the ENG stream data. Spike detection and classification in a multiunit neural recording has been an active research area in the past few decades, where many algorithms varying in complexity and performance were analyzed and used. Classifying the SFAP spikes and the exact time index where each spike occurred for each nerve single fiber would give sufficient information to determine some biomedical parameters such as muscle length and joint angles. Spike

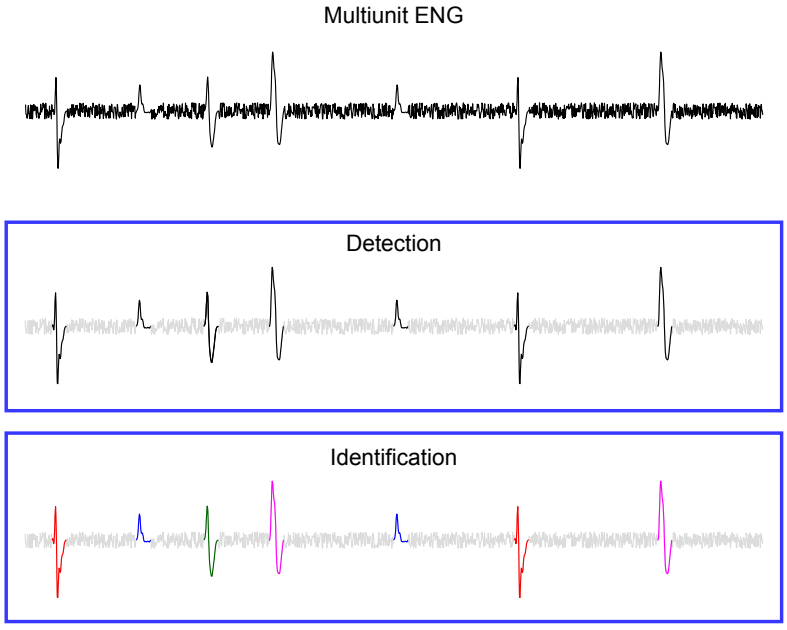

Fig. 4.1. Spike sorting procedure. Detection aims to detect any SFAP spike and identification aims to classify the detected signal based on their waveform shapes.

sorting can be divided into two major phases: detection and identification. Detection aims to detect any SFAP spike within the multiunit ENG signal. However, identification aims to separate spikes from different neurons based on their waveform shapes. Fig. 4.1 shows an example of spike detection and identification.

4.1.1 Spike Detection

Spike detection is a necessary step for spike classification devices [47]. Many spike detection algorithms have been described in the last few decades. Some of these algorithms are absolute value threshold detection (ABS) [48], nonlinear energy operator detection (NEO) [49], and matched-filter detection (MF) [50]. These methods are usually followed by a thresholding system.

Absolute Value Threshold (ABS)

ABS is the simplest detection technique that works by applying either a single threshold to detect one edge [51] of the raw data of the extracellular recording or a pair of thresholds to detect both rising and falling spike edges [52]. The threshold can be automatically set to

$$Thr = 4\sigma_N, \ where \qquad \sigma_N = median(\frac{|x(n)|}{0.6745}) \tag{4.1}$$

where $x(n)$ is input waveform and σ_N is an estimate of the standard deviation of the noise [48].

Energy Operator Detection (NEO)

NEO, also called Teager Energy Operator (TEO), results in a nonlinear approach by estimating the square of the instantaneous product of amplitude and frequency of a sufficiently sampled signal [53] as described in the following equation

$$\psi[x(n)] = x^2(n) - x(n+1) \cdot x(n-1) \tag{4.2}$$

The system considers detection when the frequency and power are large. In this case, the threshold value can be automatically set to

$$Thr = \frac{8}{N} \sum_{n=1}^{N} \psi[x(n)] \tag{4.3}$$

where N is the number of samples in the signal window.

Since this method is a non-linear approach, another effective neural signal processing demonstrator application was implemented as part of this thesis, the Matched Filter.

Matched Filter (MF)

The matched filter, type of FIR filter, is a basic correlator for detecting the presence of known wavelet template at the end of the reception of the signal in an unknown signal that contaminated with noise. This is obtained by cross-correlating the template wavelet with the unknown signal. This is performed by solving the equation

$$y(n) = \sum_{i=0}^{M} b_i x(n-i) \tag{4.4}$$

where b_i are a set of M weight values of the matched filter for an order M filter, and $x(n-i)$ represents the time signal $x(n)$ at the present time and for each $1 \cdots M$ discrete time increments in the past. $y(n)$ is the output filtered signal at time n, which its normalized output to the largest amplitude is ranged from -1 to 1 where -1, 0, and 1 indicate that the template and the unknown signal are inversely correlated, uncorrelated, and perfectly correlated respectively. The matched filter results can be obtained by averaging the expected shapes of the spike wavelets and use it as the weights of the filter. Not like other methods, the matched filter detector requires knowing the template beforehand. This detector can also work as a spike identifier as explained later.

A study concluded that NEO is slightly more effective than ABS in terms of computational complexity, but higher in cost [54]. Another study showed that the matched filter detection is as effective and accurate as ABS and NEO, but it is more complex [55]. when implemented using a DSP. In contrast, a matched filter can be readily implemented on the EAC to work not just as a detector, but as an identifier as explained later.

4.1.2 Spike Identification

The spike detection is then followed by the second phase of spike sorting that is divided into two major parts: feature extraction and clustering. Not like some detection algorithms, in most of identification approaches shape of spikes must be known beforehand. Several sorting algorithms were analyzed and used in the past few decades. Some of the most known identification algorithms are principal component analysis (PCA) [56] [57] and discrete wavelet transform (DWT) [48], for feature extraction, and fuzzy c-means (FCM) [58], the most accurate out of all clustering methods tried [59], for clustering approaches. Additionally, more methods were explored in the literature for spike identification such as neural networks (NN) [60] and matched filters. Not only the matched filter is a good detection approach as discussed before, but it is used for spike identification as well as discussed in this chapter.

Principal Component Analysis (PCA)

PCA was invented in 1901 by Karl Pearson [61]. PCA algorithm is a common technique for finding patterns in data based on eigenvalue decomposition that is usually done off-line. It performs a rotation of the data to maximize the variance of projection along each component. This is done by finding the orthogonal basis waveforms, where the waveform is linear combination of these bases. Then, only a few sets of these weights (PC), which have largest variations, usually two or three,

are considered for the clustering phase. Each spike is expressed as a series of PC coefficients C_i

$$C_i = \sum_{n=1}^{N} PC_i(n) \cdot s(n) \tag{4.5}$$

where s is the spike that consists of N samples and PC_i is the i^{th} PC.

Discrete Wavelet Transform (DWT)

DWT algorithm was first proposed by Alfred Haar [62]. It is a time-frequency representation of the signal that is similar to the Fourier Transform, but it does not only capture the frequency component of the signal, but it includes time locations as well. The signal is mapped onto the two independent variables a (scale parameter) and b (translation parameter) by performing convolution between the input signal $x(t)$ and the wavelet function described as follows

$$\psi_{a,b}(t) = \frac{1}{\sqrt{|a|}} \psi(\frac{t-b}{a}) \tag{4.6}$$

This is done by passing the input signal by a bank of quadrature mirror filter. A low-pass filter is first considered to extract the low frequency band which is called the detailed coefficients and the remaining high-frequency band is called the approximation coefficient. Same filter bank procedure is applied to detailed coefficients to create as many bands as desired. Different threshold values are then considered for each level of the detail coefficients to indicate different features for each spike. Clustering method such as FCM is then implemented to sort the spikes based on the extracted features.

Neural Network (NN)

Neural Networks are type of artificial computing intelligence that attempt to work the way a human brain works. Neural Networks are composed of many neurons

that cooperate to perform the desired function. In general, they are widely used in classification, noise reduction, and prediction. Like a human brain, Neural Network has the ability to learn and to be trained in order to do classify patterns [63]. Neural networks consist of three types of neuron layers: input, hidden, and output. The signal flow is from input to output units in a feed-forward direction. The output of a neuron is a function of the weighted sum of the inputs plus a bias. Therefore, the function of the entire neural network is simply the computation of the outputs of all the neurons. Most of the activation function used is the sigmoid function which is smooth and continuous to allow the derivative calculation which is not an option in sign function [64].

The weights of the hidden and output neurons play the major role in the classification process. These weights are calculated by training the Neural Network. Back-propagation is the most common algorithm used to train and calculate the weights of the network. This is basically done by running the network in the opposite signal flow by injecting the training pattern's target in order to generate and update the weights for a large number of iterations to allow less mean squared error (MSE).

4.1.3 Detection and Identification System with the EAC

PCA was determined to be better than DWT in terms of classification accuracy, but more computational complex [59]. Neural Network however was verified to perform slightly better than PCA [65]. But, it is very computational complex when compared to other methods. Moreover, it not only requires knowing the templates beforehand, but it also requires enormous training set for better recognition accuracy [64]. Chandra et al. reported that a trained neural network performed as well as a matched filter for classifying non-overlapping action potentials.

Besides, the matched filter is an optimal spike detector method [66]; it is used in the identification process. The matched filter, however, clusters only one unit from the data stream. Thus, several matched filters (one for each spike) need to be

implemented in order to cluster all spikes in the multiunit neural activity. Therefore, a matched filter was implemented by the EAC to not just detect ENG spikes, but to identify a target spike of the multiple units in the neural activity.

We hypothesize that the matched filter can be implemented in the EAC to accurately detect SFAP spikes, their exact timing and class of each action potential in the ENG neural activity. The matched filter by the EAC can effectively reject background noise and outcome low exclusion and inclusion errors similarly to DSPs.

4.2 Methods

Two different approaches can be taken to evaluate the matched filter classification technique and verify the stated hypothesis. One of these methods is passing an experimental multiunit neural signal recording by the designed matched filter to determine its performance; however, we are uncertain of the SFAP classes in the experimental data. Therefore, another approach was taken which is creating an artificial signal by superpositioning trains of four different spike classes, experimentally collected and processed, shown in Fig. 4.2, and contaminating them with white noise of various amplitudes that was experimentally collected as shown in Fig. 4.3. The four SFAP templates were processed from raw data that was collected from a New Zealand white rabbit by a Longitudinal Intra-Fascicular Electrode (LIFE).

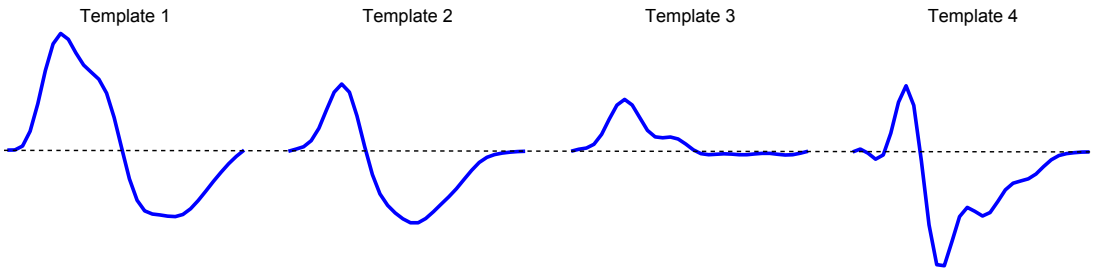

Fig. 4.2. Four different action potential templates sampled at 48 kHz used for a synthetic neural activity. Template 1 is the target unit which is the weighting function of the matched filter.

As discussed above, the voltage magnitude of the action potential represents the weighting function of the matched filter. Template 1, shown in Fig. 4.2, was selected to be the target unit that needs to be clustered in the multiunit neural activity. Thus, the weights of the target unit were defined as the FIR filters weights. The matched filter was designed in three different systems, DSP (MATLAB 2009a), FEM simulation of the EAC (COMSOL 3.5a), and a modified physical prototype of the EAC.

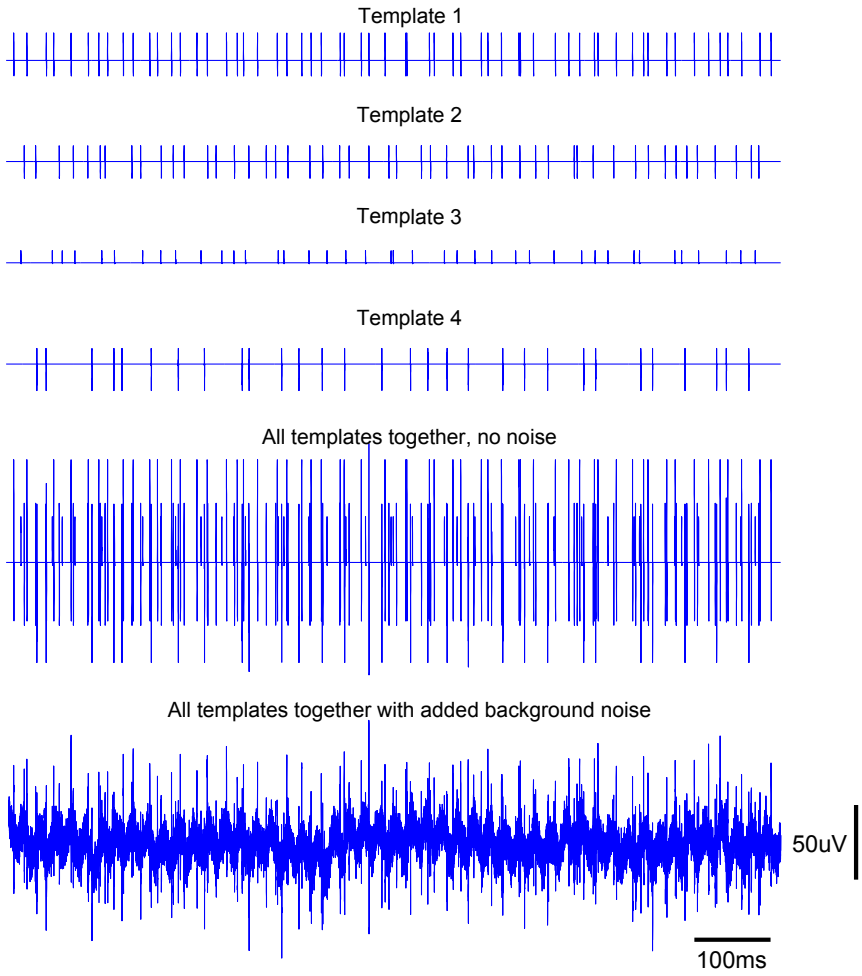

Fig. 4.3. Steps of creating a synthetic neural activity. The top 4 traces are the generated different action potential trains. The fifth trace is the superposition of traces 1-4. In the bottom trace, archived background noise is added to the generated action potential trains.

4.2.1 Matched Filter Using a DSP

Using MATLAB 2009a, a Matched filter code was designed where the weights of the filter were set to the 32-sample target action potential. The MATLAB code was designed to first accept the entire input signal and the 32-sample weights. Then, a for-loop was created to capture and sum the multiplication of every 32-sample window of the entire signal and the constant weights. The output was monitored in each iteration to represent the matched filter output. The synthesized neural multiunit signal (see Fig. 4.3) was then passed and propagated to the designed code. The output values were then normalized so that the maximum is 1. Next, a threshold value of 0.5 was set so that any value greater than the threshold value indicates the presence of the target action potential.

4.2.2 FEM Model of the Matched Filter on the EAC

The same matched filter system was also designed in the EAC using COMSOL and a physical prototype of the EAC as well. As discussed above, the voltage magnitude of the action potential characterizes the weighting function of the matched filter which includes positive and negative values. Thus, differential measurement method is used where two voltage sensors (V_1 and V_2), as shown in Fig. 4.4, were monitored at two different corners of orthogonal insulated boundaries in a conductive medium. Then, random appropriate locations of current inputs in the EAC were selected where the weighing function satisfies Eq. 3.10.

Using COMSOL 3.5a and MATLAB 2009a server link, the target single unit samples values were injected as current sources and propagated through the defined locations and the differential measurement $V_1 - V_2$ was monitored. This output was compared to the auto-correlation of the single unit to evaluate its accuracy and determine the error.

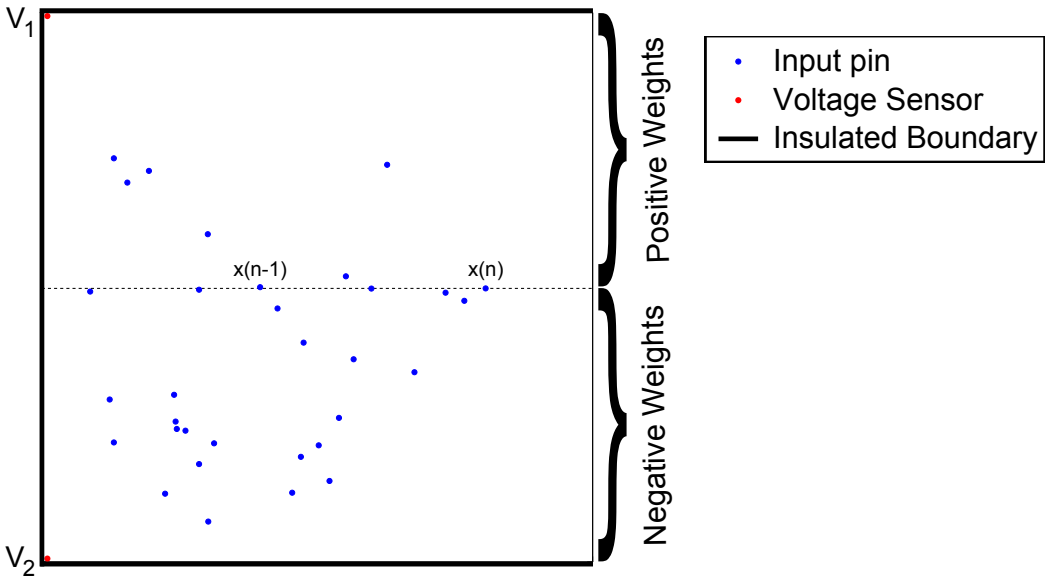

Fig. 4.4. Matched filter random configuration in the EAC for detecting the displayed single unit.

4.2.3 Physical Prototype of The EAC Implementing a Matched Filter

It was also decided to go further and implement the matched filter system with the physical prototype of the EAC. The matched filter configuration, shown in Fig. 4.4, was implemented in an 8-bit resolution prototype device, EAC R002 designed by Bryce Himebaugh at Indiana University in 2005 [67]. Using a sheet of isotropic conductive foam with conductivity of 0.1 S/m and dimensions of 11.5 $\times$ 11.5 $\times$ 0.5 cm, one side (11.5 $\times$ 0.5 cm) was grounded using two catheter needles inserted sideway opposite of each other and connected to a ground point. Then, 32 hypodermic needles were injected and arranged in the foam, as shown in Fig. 4.4, to represent the weighting function of the single unit template. The prototype EACs have only 25 pins, thus two EACs were used where the 32 input needles were connected to 25 pins of one EAC and 7 pins to the other. Both devices were connected to a computer and a Python code was created to accept two devices through USB terminals and propagate the desired 32-points input signal through the configured needles. The EAC then

injects the desired 32-points signal as electric currents. The differential measurement $V_1 - V_2$ was captured using the ultralow noise differential Amplifier (Axon Instruments AI 402 x50). The reading was then passed to another amplifier (Cyber Amp 320) and the differential measurement was monitored by a PC computer trough Mr. Kick Data Acquisition system (Sensory-Motor Interaction, Aalborg, Denmark) with a sampling frequency of 2 kHz and low-pass filter with cutoff frequency of 600 Hz. The setup is shown in Fig. 4.5. The EAC was designed to inject or measure maximum current or voltage of 200 μA and 5 V respectively for each pin. In this experiment, the EACs were only used to inject a scaled version of input signal as currents where the maximum value is 200 μA.

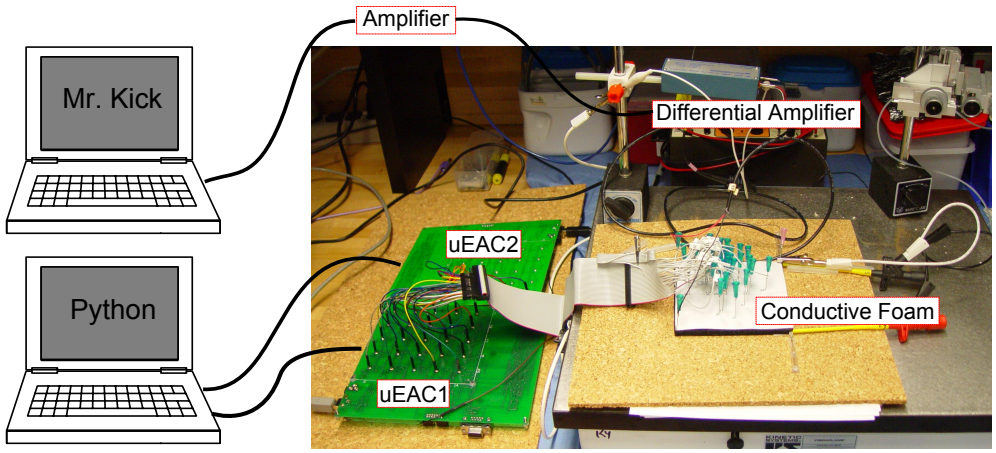

Fig. 4.5. Experiment setup to monitor the differential measurement of the matched filter configuration.

An impulse of 200 μA was injected and propagated through the input pins to measure the implemented weights of the matched filter which is the action potential single unit. The measured weights were compared to the predicted weights and percent error of each of the measured weight value was calculated. The correlation coefficient of the predicted and the measured weighting function was calculated to indicate the goodness of fit and accuracy of the implemented weights. The 32-point

target action potential unit was then injected and propagated through the 32 input pins in the matched filter configuration system by the EAC prototype and compared to the result driven by the COMSOL 3.5a of the same system.

Next, the synthesized raw neural activity, shown in Fig. 4.3, was passed through the matched filter to identify the SFAP target unit that match the template (filter weights) within the recordings. The matched filter results by the EAC prototype were then compared to the results driven by the DSP computer simulations of the EAC in order to evaluate its quality and detection accuracy.

Since background noise in neural signal is a major obstacle in the detection process, the matched filter on the EAC was further tested with various signal-to-noise ratios (SNR) of the single unit, where the noise component is peak-to-peak white noise.

4.3 Results

4.3.1 Matched Filter Using a DSP

The matched filter was able to identify the target single unit from the neural signal record. The matched filter performed remarkably well, rejecting the background noise and the lower frequency baseline oscillation while marking correctly of the instances of the nerve activities. Normalizing the matched filter data, a threshold value of approximately 0.5 was determined to achieve the best identification accuracy in terms of exclusion and inclusion errors, as shown in Fig. 4.6. The exclusion error, also known as type 1 error and false positive rate, is the probability that the system fails to detect the input templates to the target template, where the inclusion error, also known as type 2 error and false negative rate, is the probability that the system incorrectly matches the input templates to the target template. In the designed system, the exclusion error and inclusion errors were calculated to be approximately 0% and 1%, respectively.

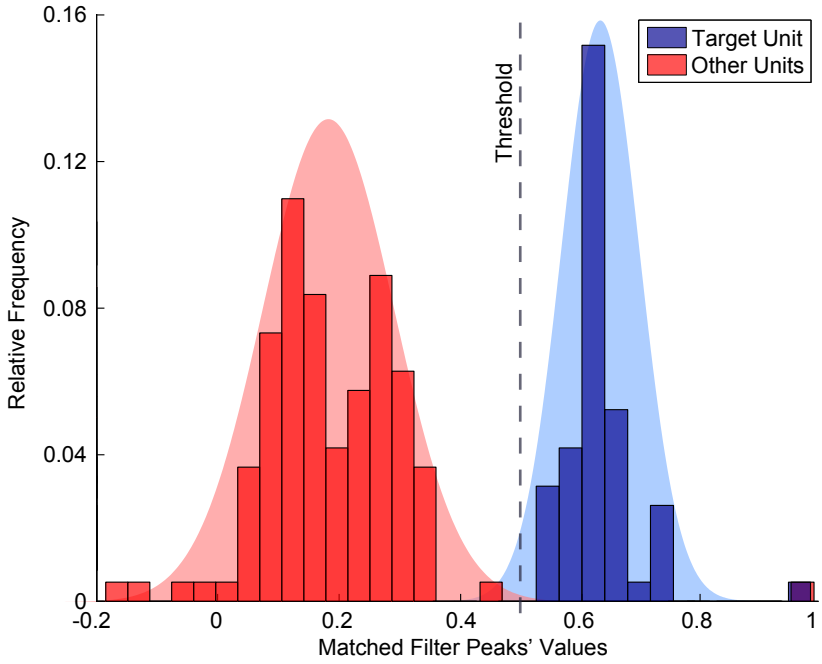

Fig. 4.6. The frequency of action potential peaks in the matched filter results. The target unit is well clustered and therefore the detection accuracy is relatively high.

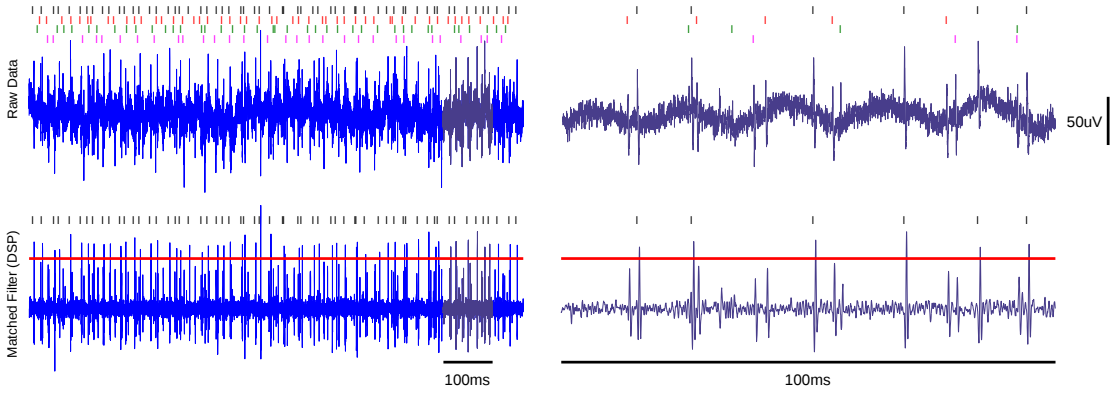

Fig. 4.7. Matched filter detector/identifier of the target unit in the raw ENG data (top) implemented with a DSP device (bottom). The right traces are a blow up of a 100 ms region of the 1 s traces (left).

4.3.2 FEM Model of the Matched Filter on the EAC

The output of injecting the target spike to the designed matched filter by the EAC through FEM simulation gives the auto-correlation function. As shown in Fig. 4.8, the output was compared to the auto-correlation of the single unit determined by MATLAB 2009a to evaluate its accuracy and determine the error. The output of the EAC simulation by FEM model matched the auto-correlation function with some error that is due to Finite Element meshing and input locations rounding error. The goodness of fit correlation was calculated to be ~ 0.9923.

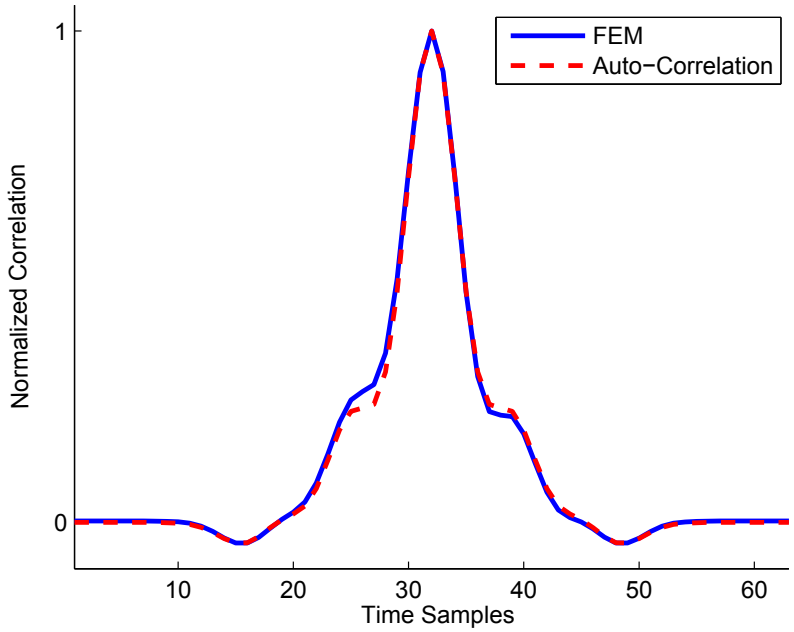

Fig. 4.8. The EAC matched filter output by COMSOL 3.5a vs. the auto-correlation function of the purified target single unit.

It is now known that the matched filter is implemented correctly in FEM model and equivalent to DSP in terms of quality and performance. Therefore, it was decided to do further analysis and verification by implementing it with a physical prototype of the EAC.

4.3.3 Physical Prototype of the EAC Implementing a Matched Filter

The measured weights were compared to the predicted weights and percent error of each of the measured weight value was calculated, shown in Fig. 4.9. The correlation coefficient of the predicted and the measured weighting function was calculated to be 0.9837 where the maximum observed percent error of the weights was less than 5%.

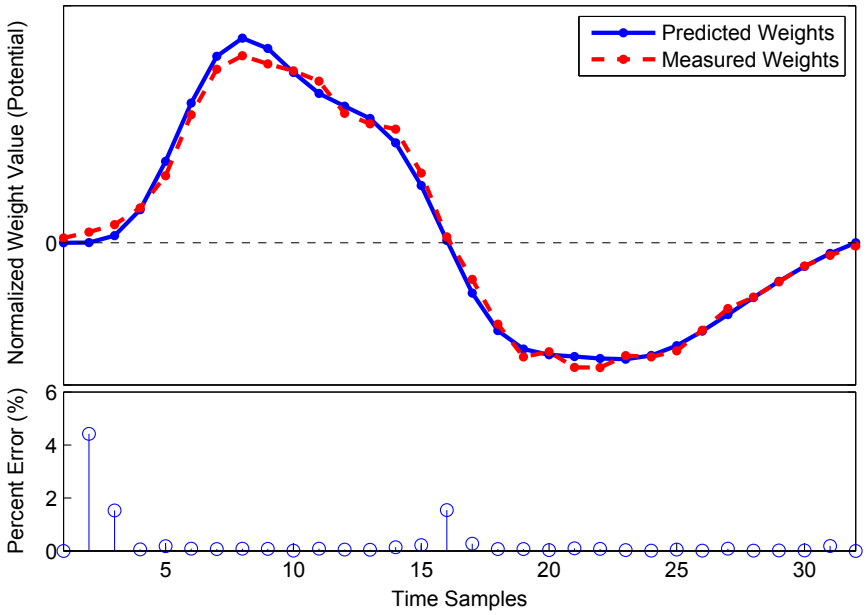

Fig. 4.9. Predicted weights implemented on the conductive foam vs. the measured weights of the target spike single unit spike.

As shown in Fig. 4.10, the target action potential injected to the matched filter system of the physical EAC prototype was compared to the FEM model of the same system. High correlation was achieved by the physical EAC prototype, however, some error was observed due to the error of the weighting function that is shown in Fig. 4.9.

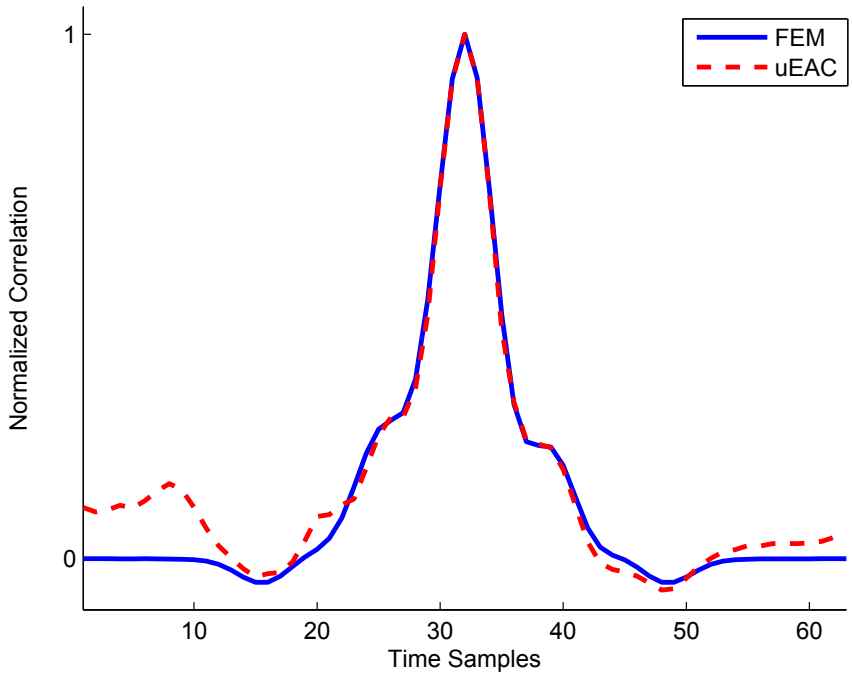

Fig. 4.10. Matched filter output resulted by FEM simulation vs. the physical EAC prototype.

As shown in Fig. 4.11, the matched filter results by the EAC prototype were equivalent to the results by the DSP computer simulations of the EAC, with a root mean square error of only 1.4%. This proves that the EAC is a reliable device and its quality is equivalent to the quality of DSPs. Even with various peak-to-peak white noise amplitudes, high detection accuracy is achieved even with low SNR values, as shown in Fig. 4.12.

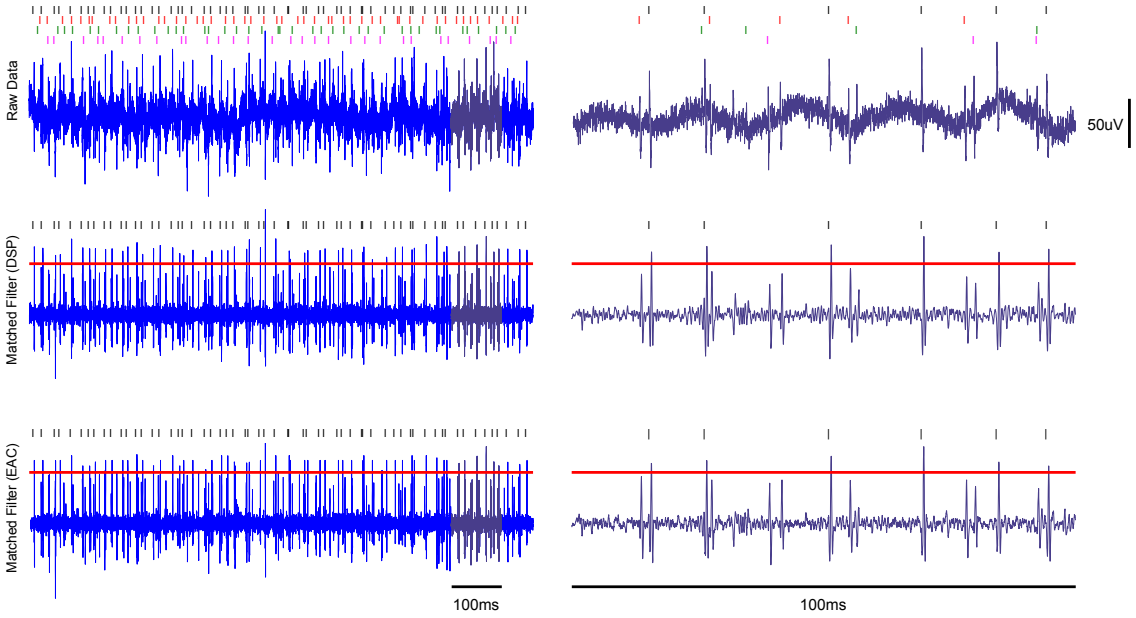

Fig. 4.11. Matched filter detector and identifier of the target unit of the raw ENG data (top) implemented with a DSP device (middle) and with EAC prototype (bottom). The right traces are a blow up of a 100 ms region of the 1 s traces (left). The quality of the matched filter by the EAC is equivalent the quality of the same filter by a DSP device.

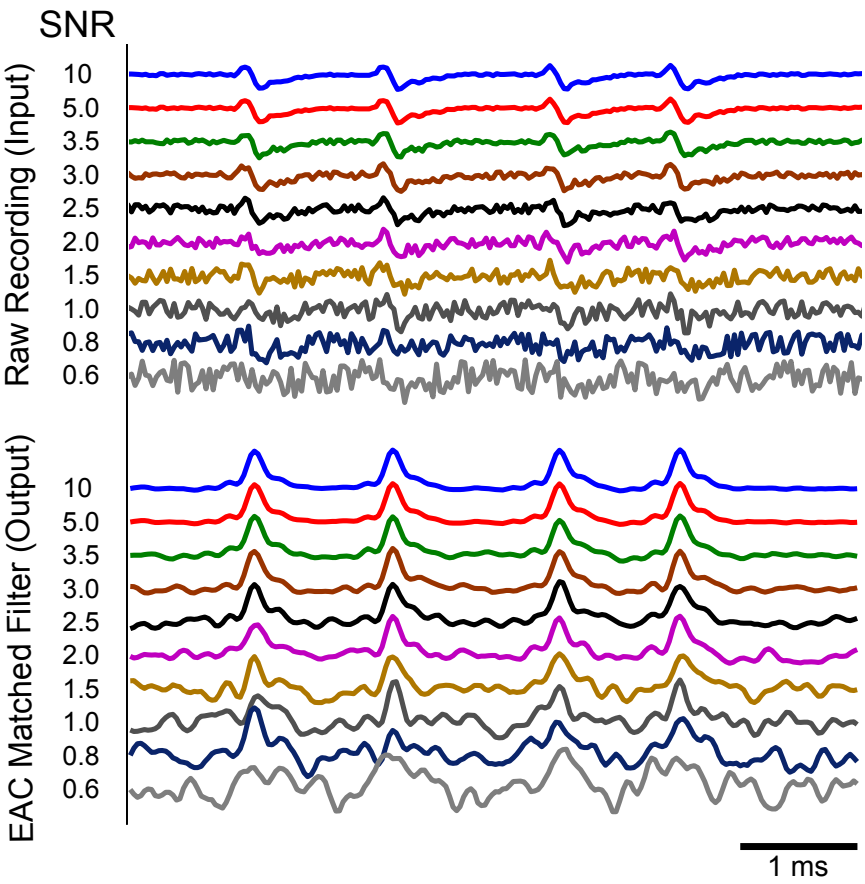

Fig. 4.12. The EAC matched filter output with different SNR values for a single unit template.

5. DISCUSSION

Real-time neural signal processing requires enormous, parallel, and fast computations. The EAC solves linear functions such as summation and multiplication effectively and nearly instantaneously. As illustrated in the reanalysis chapter, the EAC works in four different modes: current gain, voltage gain, resistance, and conductance mode, where the resistance mode was fully analyzed in this thesis. In this mode, the EAC volume conductor not only works as a summer for all inputs, but it also works as a three-dimensional series of resistors, where the distance between the current input and voltage detection point represents the reciprocal of the resistance value. This allows solving any radial bases function to possibly work as an artificial neural network. Additionally, many inputs can be injected simultaneously and parallel computations are performed.

GPAC can only solve linear PDEs, however, EAC solves not only linear PDEs, but also solves non-linear ones through LLAs that are somewhat similar to the digital logic gates, but with only one input. The EAC has also the potential to work in various neural signal processing applications such as principal component analysis and neural networks. As noticed in Eq. 4.5, the PCA clustering technique consists of only multiplication and summation, where the PC_i is considered the weighting function of an FIR filter. Using the same technique used in the matched filter, PCA can possibly be implemented on the EAC. In the neural network case, the trained weights may also be considered as the weighting function of an FIR filter to cluster the detected spikes. However, multiple EAC sheets may be connected where each sheet represents a single layer of the neural network. The training can be done using a digital computer to determine the weights in both cases: principal component analysis and neural network.

Driving the analytical solutions of different irregular designs and configurations on the EAC is a difficult task. Thus, FEM simulation becomes an important and quick technique. In this thesis, FEM platform (COMSOL 3.5a) was used to analyze the behavior of the voltage manifold in various configurations with different material characteristics. Analytical solutions are not always practical solutions and thus some assumptions and rules need to be set. For example, the analytical solution of potential manifold due to a centroid current source is under the assumption that the volume conductor is of infinite extent. Practically, this can only be achieved by grounding the boundaries of a finite volume conductor. Therefore, a 10% restricted zone is defined close to grounded boundaries where the actual solution does not perfectly match the analytical solution.

Different shapes of current sources were also analyzed to achieve an optimized shape that gives equivalent results to the analytical solution and is easy to manufacture in the meantime. It was possible to increase the potential manifold magnitudes in the volume conductor by insulating some boundaries. The insulated boundary works as a mirror wall which reflects current path in the volume conductor and subsequently, potential magnitude is doubled. The ability to compress the volume conductor and not alter the potential manifold by adjusting the conductivity parameters of x, y, and z direction was also shown.

A new approach was then developed to add a time component into the EAC so that it cannot only solve spatial differential equations, but it can also work in the time domain to work as temporal linear filters. In one configuration, the EAC implements any Finite Impulse Response (FIR) filter where the filter weights are inversely proportional to the distance between input sources and the detection point in the volume conductor. Examples of FIR filters were simulated by a prototype of the EAC, Finite Element Modeling software, and DSP computer simulation. Equivalent Results were achieved which proves the reliability of the EAC. Furthermore, an advanced configuration was shown to implement arbitrary FIR filter with positive 8-bit filter weights.

For lower order IIR systems, the EAC works well, because they are not very sensitive to coefficients. However, high order IIR filters such as 3^{rd} or 4^{th} order, are not so easy to be considered because of their greater sensitivity to their coefficients. Since the coefficients are determined by position on the EAC media, the precision in positioning of the source or observation point becomes critical. This limitation becomes critical for orders of three or more. They are very sensitive because they act on prior outputs. However, using COMSOL 3.5a, a 3^{rd} order IIR Butterworth filter was implemented on the EAC by converting the prior voltage measurements to current sources and recursing it back to the EAC volume conductor. Like the FIR filter configuration, the locations of the IIR filter tap sources and their distances to the voltage sensor represent the weights of the filter. Negligible error was determined when compared to a DSP simulation.

A major application in the neural signal processing field is detecting, identifying, and clustering SFAPs within a multiunit neural signal activity to determine the action potential rate in each nerve fiber in the nerve bundle in order to decode communication information in the body. A common algorithm for this task is the matched filter which gives the correlation value of the unknown real-time signal and the SFAP template.

Four different action potential templates were added to an archived one second of realistic background neural activity noise. These four spikes were repeated 30, 40, 50, and 60 times at random time indicies in the one second trace. Then, a matched filter for one of the four spikes was designed and implemented by a computer simulation (DSP), FEM simulation of the EAC, and a physical prototype of the EAC. Not only high classification rate was accomplished, but equivalent results were also observed when compared to each other.

Therefore, the EAC is not only equivalent to DSPs in terms of quality, but it outperforms DSPs in many other areas such as power consumption, operational speed, and ability of parallel computations to have a family of solutions simultaneously. Therefore, the EAC is a novel technique that overcomes many obstacles in the signal processing world. In the next few decades, the EAC might be developed in several

forms to solve several signal processing problems that DSPs can not solve. Moreover, the EAC has high potential to become an implantable device that can be used for neural signal processing.

5.1 Future Directions

Any order FIR or IIR filter can be implemented with the EAC; however, the higher the order of the filter, the more input taps needed and subsequently more power is required to run the system. Therefore, more simulations need to be performed to estimate the maximum filter order that can be considered for a low-power EAC. Moreover, more power would increase the temperature of the volume conductor of the EAC. Subsequently, the characteristics of the EAC volume conductor may not still be homogeneous. Therefore, the output results could be contaminated with noise which will affect the quality of the EAC.

Another idea to be considered is linking multiple EAC sheets to solve complex differential equations. As discussed before, many transfer functions and linear differential equations can be solved by the EAC. However, multiple EAC sheets can be linked so that the output sheet can be wired to an input to the next sheet. Nonlinearities can be further added by recursion of outputs back onto the manifold sheet through logic functions. This would allow solving very complicated ordinary differential equations and possibly linear algebra problems. Additionally, the conductive medium can be shaped into irregular shapes to adapt it to specific problems. Additionally, the volume conductor of the EAC has a major role in performing the calculations. Material of the volume conductors can vary and liquid materials may possibly be considered. Thus, further research would be considered to determine an optimized material for the EAC.

Furthermore, particle swarm optimization (PSO) techniques can be applied for machine learning techniques in the EAC. The change in location of sources and sinks adjusts how the current distributes itself in the space, which comes as solutions to

Poisson's equation. Once configured, the solutions to the problems posed to the EAC form nearly instantaneously, as soon as the current density distribution forms on the conductive sheet.

While EACs can perform various tasks quickly, existing EAC designs have limitations in the realm of signal processing, and more generally in the realm of processing time varying input signals. For example, adaptive signal filtering is a common task in signal processing where a filter changes dynamically to remove noise from an electromagnetic signal. Typically, the electromagnetic signal and the noise are time varying, which is to say that the values of the input signals change over time. In a traditional EAC, the time-varying input signals generate fluctuations in the electrical current flowing between sources and drains within the conductive material of the EAC. Consequently, the current density manifold within the EAC changes while the EAC is generating the solution, resulting in an unstable output. Thus, traditional EACs are often ineffective in processing time varying input signals, including adaptive filtering applications. Consequently, improvements to EACs that enable processing of time varying inputs would be beneficial.

Miniaturizing the EAC is also a major step that needs to be considered in order to form it into an implantable device. A macro size of the EAC is preferred where a sufficient number of input pins needs to be considered.

As discussed above, the EAC can work in four different modes of operation: current gain, voltage gain, resistance, and conductance mode. The current gain mode was explored previously explored by Mills et al. In this thesis, the resistance mode was explored and some applications were implemented and validated. The two other modes of operation may also by developed for signal processing tools and/or machine learning applications. Therefore, more research is needed to address these modes and potential applications that can be accomplished with them.

5.2 Summary

The EAC can be configured to do multiple mathematical operations, such as multiplication and integration, instantaneously in parallel in spatial or time domain. This allows the EAC to be a multitasking neural signal processor that solves an arbitrary linear differential equation. In the spatial domain, the potential manifold by a current source is mapped onto the conductive medium of the EAC. Then, the voltage sensor at any location in the medium becomes inversely related to the distance between the source and the sensor. Since the current source input induces high input impedance, superposition principals hold where multiple inputs can be present at the same time without altering the manifold. In this case, the voltage value at any location on the EAC indicates the weighted sum of the source values where the weights are inversely proportional to the distances between the sources and the voltage sensor.

In the time domain, a sampled time signal is mapped to the distance axis of the EAC as current sources so that the voltage sensor value corresponds to the weighted sum of the input data samples. In other words, the voltage sensor represents the FIR filter output where the inverse of the distances between the input sources and the voltage sensor represents the weights of the filter. These weights can be tuned by tuning the locations of input sources to implement the desired FIR filter.

Moreover, IIR filters can be implemented with the EAC by recursing the detected output voltage back as a current input using a transconductance amplifier for next sample calculations. In this case, the inverse of the distance between the recursed value locations and the output of the IIR filter represents the feedback coefficients of the filter. This would allow solving any linear differential equation by finding appropriate locations of the feedforward and feedback coefficients. This concept was validated by implementing FIR and IIR filters. It was further validated with a practical neural processing application, matched filter, for detecting and classifying SFAP spikes within neural data stream. A synthesized signal was created by contaminating a train of four different templates with realistic measured neural background noise.

The EAC showed equivalent results to DSP simulation while low exclusion and inclusion errors were determined. This proves that the EAC is a reliable device that is capable to replace and even outperforms DSPs in many extents such as power consumption and parallel computing.

6. CONCLUSIONS

Digital and analog computers have advantages and disadvantages. The EAC, however, combines the advantages of both analog and digital computers. A classical digital computer reconfigures itself quickly to answer new questions by loading software and performing the algorithms in the software. However, certain types of questions are difficult for digital computers to solve in reasonable amounts of time. As shown, the EAC can perform the equivalent computations of a complex digital simulation much more efficiently than a digital computer.

The EAC is not only a parallel analog processor with massive computational capacity, but it is also a digitally configurable and a low power device. Therefore, the EAC has high potential of being an efficient implantable neural signal processor. In this thesis, it was proven that the EAC can efficiently work as an FIR, IIR filters, or a combination of both. To prove the quality of the EAC, a matched filter, an example of FIR filter, was simulated by a prototype of the EAC and compared to digital computer simulation, where equivalent results were observed. Therefore, the EAC is a radically different and high performance computing technique that would address the technological gap for mobile neural signal processing and provide richer processed information than current computing techniques.

LIST OF REFERENCES

LIST OF REFERENCES

[1] K. Yoshida, D. Farina, M. Akay, and W. Jensen, "Multichannel Intraneural and Intramuscular Techniques for Multiunit Recording and Use in Active Prostheses," *Proceedings of the IEEE*, vol. 98, pp. 432 –449, March 2010.

[2] K. Yoshida and K. Horch, "Closed-loop control of ankle position using muscle afferent feedback with functional neuromuscular stimulation," *Biomedical Engineering, IEEE Transactions on*, vol. 43, pp. 167 –176, February 1996.

[3] K. Yoshida, K. Jovanovic, and R. Stein, *Developments in longitudinal intrafascicular electrodes for peripheral nerve recording and stimulation*, pp. 1661, No. 652.7. 1998.

[4] R. Stein, T. Nichols, J. Jhamandas, L. Davis, and D. Charles, "Stable long-term recordings from cat peripheral nerves," *Brain Research*, vol. 128, no. 1, pp. 21 – 38, 1977.

[5] S. Qiao and K. Yoshida, "Influence of unit distance and conduction velocity on the spectra of extracellular action potentials recorded with intrafascicular electrodes," *Medical Engineering and Physics*, 2012.

[6] N. Ganapathy and J. Clark, "Extracellular currents and potentials of the active myelinated nerve fiber," *Biophysical Journal*, vol. 52, no. 5, pp. 749 – 761, 1987.

[7] N. Dalkilic and F. Pehlivan, "Comparison of fiber diameter distributions deduced by modeling compound action potentials recorded by extracellular and suction techniques," *International Journal of Neuroscience*, vol. 112, no. 8, p. 913, 2002.

[8] G. L. Gerstein and W. A. Clark, "Simultaneous Studies of Firing Patterns in Several Neurons," *Science*, vol. 143, no. 3612, pp. 1325–1327, 1964.

[9] T. McNaughton and K. Horch, "Action potential classification with dual channel intrafascicular electrodes," *Biomedical Engineering, IEEE Transactions on*, vol. 41, pp. 609 –616, July 1994.

[10] K. Yoshida and R. Stein, "Characterization of signals and noise rejection with bipolar longitudinal intrafascicular electrodes," *Biomedical Engineering, IEEE Transactions on*, vol. 46, pp. 226 –234, February 1999.

[11] K. Yoshida, K. Hennings, and S. Kammer, "Acute Performance of the Thin-Film Longitudinal Intra-Fascicular Electrode," in *Biomedical Robotics and Biomechatronics, 2006. BioRob 2006. The First IEEE/RAS-EMBS International Conference on*, pp. 296 –300, February 2006.

[12] Texas Instruments Incorporated, *TMS320C6746 Fixed/Floating-Point DSP*, October 2011.

[13] L. A. Rubel, "The extended analog computer," *Advances in Applied Mathematics*, vol. 14, pp. 39–50, March 1993.

[14] J. W. Mills, "The nature of the Extended Analog Computer," *Physica and Nonlinear Phenomena*, vol. 237, no. 9, pp. 1235 – 1256, 2008.

[15] J. Kennedy and R. Eberhart, "Particle swarm optimization," in *Neural Networks, 1995. Proceedings., IEEE International Conference on*, vol. 4, pp. 1942 –1948 vol.4, November/December 1995.

[16] J. W. Mills, "The continuous retina: image processing with a single-sensor artificial neural field network," in *Neural Networks, 1996., IEEE International Conference on*, vol. 2, pp. 886 –891 vol.2, June 1996.

[17] D. S. Graça and J. F. Costa, "Analog computers and recursive functions over the reals," *Journal of Complexity*, vol. 19, pp. 644–664, 2003.

[18] C. Shannon, "Mathematical theory of the differential analyzer," *Journal of Mathematics and Physics MIT*, vol. 20, pp. 337–354, 1941.

[19] M. B. Pour-El, "Abstract computability and its relation to the general purpose analog computer (some connections between logic, differential equations and analog computers)," *Transactions of the American Mathematical Society*, vol. 199, pp. 1–28, 1974.

[20] L. Lipshitz and L. A. Rubel, "A differentially algebraic replacement theorem and analog computability," *Proceedings of the American Mathematical Society*, vol. 99, pp. 367–372, 1987.

[21] D. S. Graça, M. L. Campagnolo, and J. Buescu, "Robust simulations of turing machines with analytic maps and flows," in *CiE 2005: New Computational Paradigms, LNCS 3526*, pp. 169–179, Springer, 2005.

[22] A. M. Turing, "On Computable Numbers, with an Application to the Entscheidungs problem," *Proceedings of the London Mathematical Society*, vol. 42, pp. 230–265, 1937.

[23] L. A. Rubel, "The brain as an analog computer," *Journal of Theoretical Neurobiology*, vol. 4, pp. 73–81, 1985.

[24] J. W. Mills, M. Parker, B. Himebaugh, C. Shue, B. Kopecky, and C. Weilemann, ""Empty Space" Computes: The Evolution of an Unconventional Supercomputer," *Computer Science Department, School of Informatics, Indiana University, Bloomington, Indiana*, May 2006.

[25] V. Belevitch, "Summary of the History of Circuit Theory," *Proceedings of the IRE*, vol. 50, pp. 848 –855, May 1962.

[26] R. Eberhart, J. Mills, B. Himebaugh, and X. Hu, "Method and apparatus for evolving overlays to operate an extended analog computer as a classifier or a controller," February 2010.

[27] W. Karplus, *Analog simulation: solution of field problems*. McGraw-Hill series in information processing and computers, McGraw-Hill, 1958.

[28] J. Small, *The Analogue Alternative: The Electronic Analogue Computer in Britain and the USA, 1930-1975*. Studies in the history of science, technology, and medicine, Routledge, 2001.

[29] S. Softky and J. Jungerman, "Electrolytic Tank Measurements in Three Dimensions," *Review of Scientific Instruments*, vol. 23, no. 6, pp. 306–307, 1952.

[30] A. Boothroyd, E. Cherry, and R. Makar, "An electrolytic tank for the measurement of steady-state response, transient response, and allied properties of networks," *Proceedings of the IEE - Part I: General*, vol. 96, pp. 163 –177, May 1949.

[31] W. G. Adams, "The Bakerian Lecture: On the Forms of Equipotential Curves and Surfaces and Lines of Electric Force.," *Proceedings of the Royal Society of London*, vol. 23, no. 156-163, pp. 280–284, 1874.

[32] D. C. DePackh, "A Resistor Network for the Approximate Solution of the Laplace Equation," *Review of Scientific Instruments*, vol. 18, no. 10, pp. 798–799, 1947.

[33] S. C. Redshaw, "An Electrical Potential Analyser," *Proceedings of the Institution of Mechanical Engineers*, vol. 159, no. 1, pp. 55–80, 1948.

[34] A. Cheng and D. Cheng, "Heritage and early history of the boundary element method," *Engineering Analysis with Boundary Elements*, vol. 29, pp. 268–302, March 2005.

[35] M. Buhmann, *Radial Basis Functions: Theory and Implementations*. Cambridge Monographs on Applied and Computational Mathematics, Cambridge University Press, 2003.

[36] J. Malmivuo and R. Plonsey, *Bioelectromagnetism : Principles and Applications of Bioelectric and Biomagnetic Fields*. Oxford University Press, USA, 1 ed., July 1995.

[37] S. Grimnes and O. G. Martinsen, "Chapter6 - Geometrical Analysis," in *Bioimpedance and Bioelectricity Basics (Second Edition)*, pp. 161 – 204, New York: Academic Press, second edition ed., 2008.

[38] P. Horowitz and W. Hill, *The Art of Electronics*. Cambridge University Press, 1989.

[39] A. Oppenheim, A. Willsky, and S. Nawab, *Signals and systems*. Prentice-Hall signal processing series, Prentice Hall, 1997.

[40] N. Wiener, *Extrapolation, Interpolation, and Smoothing of Stationary Time Series with Engineering Applications*. The M.I.T. Paperback series, M.I.T. Press, 1949.

[41] F. Becker, L. Holzman, R. Lucky, and E. Port, "Automatic equalization for digital communication," *Proceedings of the IEEE*, vol. 53, pp. 96 – 97, January 1965.

[42] K. R. Betty and G. Horlick, "Transversal filtering of analog signals with a tapped analog delay line," *Analytical Chemistry*, vol. 48, no. 14, pp. 2248–2252, 1976.

[43] J. J. Struijk, "The extracellular potential of a myelinated nerve fiber in an unbounded medium and in nerve cuff models," *Biophysical Journal*, vol. 72, no. 6, pp. 2457 – 2469, 1997.

[44] H. von Helmholtz, *Ueber einige Gesetze der Vertheilung elektrischer Ströme in körperlichen Leitern mit Anwendung auf die thierisch-elektrischen Versuche.* 1853.

[45] L. N. S. Struijk, M. Akay, and J. J. Struijk, "The Single Nerve Fiber Action Potential and the Filter Bank - A Modeling Approach," *Biomedical Engineering, IEEE Transactions on*, vol. 55, pp. 372 –375, January 2008.

[46] W. Thomson, "Delay networks having maximally flat frequency characteristics," *Journal of the Institution of Electrical Engineers*, vol. 1949, p. 305, December 1949.

[47] R. N. McDonough and A. D. Whalen, *Detection of Signals in Noise.* Orlando, FL, USA: Academic Press, Inc., 1995.

[48] R. Q. Quiroga, Z. Nadasdy, and Y. Ben-Shaul, "Unsupervised Spike Detection and Sorting with Wavelets and Superparamagnetic Clustering," *Neural Computation*, vol. 16, no. 8, pp. 1661 – 1687, 2004.

[49] S. Mukhopadhyay and G. Ray, "A new interpretation of nonlinear energy operator and its efficacy in spike detection," *Biomedical Engineering, IEEE Transactions on*, vol. 45, pp. 180 –187, February 1998.

[50] I. Obeid and P. Wolf, "Evaluation of spike-detection algorithms fora brain-machine interface application," *Biomedical Engineering, IEEE Transactions on*, vol. 51, pp. 905 –911, June 2004.

[51] S. Gozani and J. Miller, "Optimal discrimination and classification of neuronal action potential waveforms from multiunit, multichannel recordings using software-based linear filters," *Biomedical Engineering, IEEE Transactions on*, vol. 41, pp. 358 –372, April 1994.

[52] K. Guillory and R. Normann, "A 100-channel system for real time detection and storage of extracellular spike waveforms," *Journal of Neuroscience Methods*, vol. 91, no. 1-962, pp. 21 – 29, 1999.

[53] J. Kaiser, "Ona simple algorithm to calculate the 'energy' of a signal," in *Acoustics, Speech, and Signal Processing, 1990. ICASSP-90., 1990 International Conference on*, pp. 381 –384 vol.1, April 1990.

[54] S. Gibson, J. Judy, and D. Markovic, "Technology-Aware Algorithm Design for Neural Spike Detection, Feature Extraction, and Dimensionality Reduction," *Neural Systems and Rehabilitation Engineering, IEEE Transactions on*, vol. 18, pp. 469 –478, October 2010.

[55] K. H. Kim and S. J. Kim, "A wavelet-based method for action potential detection from extracellular neural signal recording with low signal-to-noise ratio," *Biomedical Engineering, IEEE Transactions on*, vol. 50, pp. 999 –1011, August 2003.

[56] D. A. Adamos, E. K. Kosmidis, and G. Theophilidis, "Performance evaluation of PCA-based spike sorting algorithms," *Computer Methods and Programs in Biomedicine*, vol. 91, no. 3, pp. 232 – 244, 2008.

[57] M. S. Lewicki, "A review of methods for spike sorting: the detection and classification of neural action potentials," *Network: Computation in Neural Systems*, vol. 9, no. 4, pp. 53–78, 1998.

[58] K. H. Kim, "A Fully-Automated Neural Spike Sorting Based on Projection Pursuit and Gaussian Mixture Model," in *Neural Engineering, 2005. Conference Proceedings. 2nd International IEEE EMBS Conference on*, pp. 151 –154, March 2005.

[59] S. Gibson, J. W. Judy, and D. Markovic, "Comparison of spike-sorting algorithms for future hardware implementation," in *Engineering in Medicine and Biology Society, 2008. EMBS 2008. 30th Annual International Conference of the IEEE*, pp. 5015 –5020, August 2008.

[60] K. H. Kim and S. J. Kim, "Neural spike sorting under nearly 0-dB signal-to-noise ratio using nonlinear energy operator and artificial neural-network classifier," *Biomedical Engineering, IEEE Transactions on*, vol. 47, pp. 1406 –1411, October 2000.

[61] K. Pearson, "On lines and planes of closest fit to systems of points in space," *Philosophical Magazine*, vol. 2, no. 6, pp. 559–572, 1901.

[62] A. Haar, "Zur Theorie der orthogonalen Funktionensysteme," *Mathematische Annalen*, vol. 69, pp. 331–371, 1910.

[63] J. J. Hopfield, "Neurocomputing: foundations of research," ch. Neural networks and physical systems with emergent collective computational abilities, pp. 457–464, Cambridge, MA, USA: MIT Press, 1988.

[64] R. Duda, P. Hart, and D. Stork, *Pattern classification*. Pattern Classification and Scene Analysis: Pattern Classification, Wiley, 2001.

[65] L. J. Trejo and M. J. Shensa, "Linear and neural network models for predicting human signal detection performance from event-related potentials: A comparison of the wavelet transform with other feature extraction methods," in *Society for Computer Simulation*, pp. 153–161, 1993.

[66] E. N. Kamavuako, W. Jensen, K. Yoshida, M. Kurstjens, and D. Farina, "A criterion for signal-based selection of wavelets for denoising intrafascicular nerve recordings," *Journal of Neuroscience Methods*, vol. 186, no. 2, pp. 274 – 280, 2010.

[67] B. Himebaugh, "Design of EAC R002." http://www.cs.indiana.edu/∼bhimebau, 2005. Last accessed July 2012.